Two separate roles for the transcription coactivator SAGA and a set of genes redundantly regulated by TFIID and SAGA

Rafal Donczew [1*], Linda Warfield[1*], Derek Pacheco[1], Ariel Erijman[1,2] and Steven Hahn[1$]

* Equal contributions

[1]Fred Hutchinson Cancer Research Center,

1100 Fairview Ave N. A1-162, Seattle, WA 98109

[2] Present address: New England Biolabs, Ipswich, MA 01938

[$]Correspondence to Steven Hahn, shahn@fredhutch.org, 206 667 5261

Abstract

Deletions within genes coding for subunits of the transcription coactivator SAGA caused strong genome-wide defects in transcription and SAGA-mediated chromatin modifications. In contrast, rapid SAGA depletion produced only modest transcription defects at 13% of protein-coding genes – genes that are generally more sensitive to rapid TFIID depletion. However, transcription of these “coactivator-redundant” genes is strongly affected by rapid depletion of both factors, showing the overlapping functions of TFIID and SAGA at this gene set. We suggest that this overlapping function is linked to TBP-DNA recruitment. The remaining 87% of expressed genes that we term “TFIID-dependent” are highly sensitive to rapid TFIID depletion and insensitive to rapid SAGA depletion. Genome-wide mapping of SAGA and TFIID found binding of both factors at many genes independent of gene class. DNA analysis suggests that the distinction between the gene classes is due to multiple components rather than any single regulatory factor or promoter sequence motif.

Efficient in vitro transcription by RNA Polymerase II (Pol II) is initiated with six basal transcription factors (TATA binding protein (TBP), TFIIA, TFIIB, TFIIE, TFIIF, TFIIH), Pol II enzyme and TATA-containing promoter DNA. Cellular mRNA transcription, much of which initiates at non-TATA-containing promoters, also requires one or more coactivator complexes such as Mediator, TFIID, SAGA, NuA4 and Swi/Snf, that either directly contact the basal transcription machinery and/or modify chromatin (Allen and Taatjes, 2015; Doyon and Côté, 2004; Hahn and Young, 2011; Hantsche and Cramer, 2017; Nogales et al., 2017; Rando and Winston, 2012; Sainsbury et al., 2015). Often recruited by transcription activators, coactivators play roles in processes such as promoter recognition, assembly of the basal factors into a functional preinitiation complex (PIC), catalysis of covalent chromatin modifications, nucleosome positioning, and stimulation of early steps in the transition from transcription initiation to elongation. Although we know much about the structure, enzymatic functions, and protein-protein interactions among many of the above factors, relatively little is known about mechanisms that determine genome-wide coactivator specificity and the molecular mechanisms of how they promote induction and maintenance of activated transcription.

The yeast coactivators SAGA and TFIID share five subunits (Grant et al., 1998) but are otherwise unrelated. SAGA contains four known activities: activator binding, histone H3-acetylation, histone H2B deubiquitylation and TBP binding (Han et al., 2014; Helmlinger et al., 2011; Lee et al., 2011; Liu et al., 2019; Setiaputra et al., 2015). In addition to performing chromatin modifications, SAGA was recently shown to function as a TBP-DNA loading factor, mediated in part via TFIIA and its TBP-binding subunit Spt3 (Papai et al., 2019). TFIID is a large dynamic complex, comprised of TBP and 13-14 Taf (TBP associated factor) subunits, that functions in activator binding, promoter recognition and PIC formation (Bieniossek et al., 2013; Hahn and Young, 2011; Nogales et al., 2017). Prior studies showed that TFIID can bind one or more short downstream metazoan promoter elements and that it undergoes large conformational changes while positioning TBP on DNA (Kolesnikova et al., 2018; Louder et al., 2016). CryoEM structures of human TFIID and TFIIA-TFIID-DNA revealed that this complex seems incompatible with PIC formation (Patel et al., 2018). Several Tafs in the TFIID-DNA complex are in position to clash

with TFIIF and Pol II in the PIC and the DNA bend in the TFIIA-TFIID-DNA complex is different from that in the closed state PIC. From this it was proposed that TFIID, in conjunction with TFIIA, functions as a TBP-loading factor and that the Tafs must either dissociate or undergo major rearrangement before PIC assembly (Joo et al., 2017; Patel et al., 2018).

The genome-wide promoter specificities of SAGA and TFIID have been the subject of much investigation. Early work showed that at least some yeast genes can be activated and transcribed after depletion or inactivation of TFIID (Taf) subunits (Kuras et al., 2000; Li et al., 2000; Moqtaderi et al., 1996; Walker et al., 1996). Pioneering genome-wide studies later suggested that both TFIID and SAGA contribute to steady state mRNA expression of most yeast genes, but that transcription of nearly all genes is dominated by the dependence on either TFIID or SAGA (Huisinga and Pugh, 2004). From this study, the “TFIID-dominated” class represented ~90% of Pol II-transcribed genes, many of which lacked a consensus TATA element, while the “SAGA-dominated” genes are enriched for TATA-containing and stress-inducible genes. Formaldehyde crosslinking methods showed that promoters from the TFIID-dominated class generally have high levels of TFIID-subunit crosslinking while lower levels of crosslinking are often observed at the SAGA-dominated genes (Kuras et al., 2000; Li et al., 2000; Rhee and Pugh, 2012).

Several subsequent findings challenged these initial models. First, mutations affecting genome-wide transcription are now known to alter mRNA stability, making prior steady state mRNA measurements used in earlier studies of TFIID and SAGA specificity problematic (Haimovich et al., 2013; Munchel et al., 2011; Sun et al., 2012). Second, mapping SAGA-dependent chromatin modifications showed that SAGA modifies chromatin at nearly all expressed genes, rather than only at the SAGA-dominated subset (Bonnet et al., 2014). Third, formaldehyde-independent mapping of SAGA and TFIID using the MNase-based ChEC-seq approach identified TFIID and SAGA binding at both gene classes (Baptista et al., 2017; Grünberg et al., 2016). Finally, native Pol II ChIP and/or analysis of newly synthesized mRNA found that the majority of genes showed decreased transcription upon deletion or depletion of SAGA or TFIID subunits (Baptista et al.,

2017; Warfield et al., 2017). However, the proposal that TFIID is generally required for transcription was recently disputed based on anchor-away depletion of the TFIID subunit Taf1 (Petrenko et al., 2019). Analysis of the top 10% of transcribed genes, analyzed by Pol II-ChIP, showed that many genes in the SAGA-dominated class were only modestly sensitive to Taf1 depletion.

We have now investigated the genome-wide specificities of TFIID and SAGA by monitoring levels of newly synthesized RNA after rapid TFIID and SAGA depletion. This approach has greater sensitivity and lower background than methods used in earlier studies and allows reliable quantitation of mRNAs for ≥83% of yeast genes after factor depletion. We find that SAGA has two separable functions in gene expression: (1) a general function important for transcription of nearly all genes. This function was revealed by deletions in genes encoding key SAGA subunits. (2) a gene-specific role revealed by rapid depletion of SAGA function, where only 13% of genes are modestly affected. Surprisingly, this smaller gene set is, on average, more sensitive to rapid TFIID depletion. These and other results suggest that TFIID and SAGA function is substantially redundant at this set of co-regulated genes that we term "coactivator-redundant" rather than "SAGA-dominated" or "Taf-independent" as previously proposed. The other 87% of yeast genes that we term "TFIID-dependent" are very sensitive to rapid TFIID depletion but show little or no change upon rapid SAGA depletion. We further found that the role of SAGA in global transcription is strongly linked to SAGA-dependent chromatin modifications, particularly Gcn5-dependent H3 acetylation. This mark, that we find is required for efficient global transcription, is significantly reduced in the *SPT* deletions but declines only slowly in the rapid depletion experiments. Finally, we examine features that distinguish the two gene sets and the role of SAGA in maintenance of ongoing activated transcription at the coactivator-redundant genes.

Results

SAGA has two separate roles in transcription

To investigate the basis for conflicting reports on the genome-wide roles of SAGA and TFIID, we used 4-thioU RNA-seq to quantitate transcriptional changes that are caused by various SAGA depletion strategies. Yeast were grown in synthetic or rich glucose media and RNAs labeled for 5 min, followed by purification of the labeled RNA and quantitation by sequencing. This method has much higher sensitivity and lower background compared with Pol II ChIP and allows reproducible quantitation of newly-synthesized mRNA from ≥83% of Pol II-transcribed genes (Methods). Experiments, except where noted, were performed in triplicate and there was low variation across the set of analyzed genes (**Fig S1A, B**).

We examined genome-wide transcription changes caused by deletions in the SAGA subunits: *spt3Δ*, *spt7Δ*, or *spt20Δ* or by rapid depletion of several SAGA subunits using the auxin-degron system (Nishimura et al., 2009). To increase the probability of efficient SAGA inactivation, double degron strains permitted simultaneous depletion of two SAGA subunits, either Spt3/7 or Spt3/20. Spt3 is important for TBP binding and DNA loading while Spt7 and Spt20 are important for the integrity of SAGA (Han et al., 2014; Lee et al., 2011; Liu et al., 2019; Papai et al., 2019; Sterner et al., 1999). The depletion by degron approach was also applied to the individual TFIID subunits Taf1, Taf7 and Taf13 that are located in two different TFIID lobes (Patel et al., 2018; Warfield et al., 2017). Protein degradation was induced by adding the auxin indole-3-acetic acid (IAA) for 30 min, after which time, ≤10% of protein remained (**Fig S2A, B**). In the degron strains, mRNA levels from nearly all genes in the absence of IAA was within ~20% of that from WT strains lacking a degron (**Fig S3A**) and addition of IAA to a WT strain had no effect on gene expression (see below).

We found a striking difference in genome-wide transcription defects when comparing rapid inactivation of SAGA, a strain containing an *SPT3* deletion, or rapid inactivation of Taf13 (**Fig 1A, Tables S1, S2**). For example, the *spt3Δ* strain showed strong genome-wide transcription defects for nearly all genes while degron-induced inactivation of Spt3/Spt20 for 30 min caused only modest defects at a small subset of genes. The strong decrease in genome-wide transcription in the *SPT* deletion strains is in good agreement with prior results obtained using dynamic

transcriptome analysis (DTA) and 4-thioU-labeled RNA (Baptista et al., 2017). Rapid depletion of Taf13, a key TBP-interacting subunit located in TFIID lobe A, caused strong genome-wide transcription defects at most genes as previously observed using native Pol II ChIP (Warfield et al., 2017). For all strains assayed, the changes in gene expression showed poor correlation with a stress-response transcription signature (O'Duibhir et al., 2014), indicating that the changes we observed are not due to a general stress response (**Fig S4A**). The degron-containing strains showed ≥85% viability after 30 min of IAA treatment (**Fig S4B**) (Warfield et al., 2017).

To determine whether subsets of genes are differentially affected by any of these depletion strategies, the $\log_2$ change in transcription values from the SAGA deletion strains and TFIID-degron strains were clustered by k-means algorithm with the results shown in **Fig 1B** and **Table S3**. Grouping into two clusters showed that the two sets of genes respond differently to TFIID or SAGA depletion. The clustering was very robust as we obtained >95% overlap in gene categories when we clustered using results from the SAGA-degron strains instead of the *SPT* deletion strains. The largest cluster, we term "TFIID-dependent genes" (see reasoning below), contains 87% of analyzed genes (4245 genes) and is most sensitive to TFIID depletion. These genes show a ~4.5-fold average decrease in transcription upon depletion of ether Taf13, Taf7 or Taf1 (**Fig 2A)**, orange boxes, lanes 8-11). Results for the Taf13-degron are very similar when cells are grown in either synthetic complete (SC) or rich (YPD) glucose media with excellent correlations between Taf1, 7 and 13 depletions (**Fig S4C**). This large gene set was also sensitive to gene deletions in SAGA subunits with genome-wide transcription decreased by an average of ~2.7-fold in the *spt3Δ* strain with lesser but significant defects observed in the *spt7Δ* and *spt20Δ* strains (**Fig 2A**, orange boxes, lanes 5-7). In contrast, expression of nearly all genes in the "TFIID-dependent" set showed little or no change upon rapid SAGA subunit depletion using the Spt3/20 and Spt3/7 degron strains (**Fig 2A,** orange boxes, lanes 2-4).

The smaller gene set, that we term "TFIID/SAGA-redundant" (or "coactivator-redundant" (CR); see reasoning below), contains 13% of analyzed genes (655 genes) and these genes are more sensitive to deletions in SAGA subunits (~3-4-fold decrease) and less sensitive to TFIID depletion

(~1.5-2-fold decrease) compared with the TFIID-dependent genes. (**Fig 2A**, blue boxes, lanes 5-11). Surprisingly, these coactivator-redundant genes showed only modest transcription defects upon rapid SAGA depletion (**Fig 2A**, blue boxes, lanes 2-7). The strongest average defect was caused by the Spt3/20 degron, with an average transcription decrease of ~1.6-fold. Combined, our results show that there is a fundamental difference between cell growth for many generations in the absence of SAGA vs rapid depletion of SAGA function. Surprisingly, comparison of transcription defects caused by rapid TFIID depletion vs rapid SAGA depletion showed that the coactivator-redundant genes are, on average, more sensitive to rapid depletion of TFIID (**Fig 2A**, blue boxes, lanes 2-4; 8-11). For example, we observed a ~2-fold average decrease in transcription in the Taf13-degron vs ~1.6-fold decrease in the Spt3/20 degron.

The results above show that transcription of the smaller gene set is not dominated by either coactivator and suggests that TFIID and SAGA function is at least partially redundant at these genes. To quantitate the extent of TFIID and SAGA redundancy at all genes, we rapidly depleted both TFIID and SAGA using Taf13/Spt3 and Taf13/Spt7 double degron strains. We found that simultaneous TFIID and SAGA depletion causes a severe defect in the coactivator-redundant gene set with an average decrease of ~5.7-fold (**Fig 2B**, blue boxes, lanes 4-5; **Fig 2C**, **Fig S5A** left panel, and **Table S4**). For nearly all these genes, the transcription defect is greater than simply the sum of the defects observed in the Taf13-degron and Spt3/20-degron (**Fig S5B**), showing that there is substantial redundancy in the ability of TFIID and SAGA to promote transcription of these genes. In contrast, the TFIID-dependent genes show, on average, no additional defects in the double degron strains compared with the Taf13-degron (**Fig 2B**, orange boxes, lanes 3-5); **Fig S5A** right panel, and **Table S4**).

After 30 min of IAA treatment, the levels of each degron-tagged Spt subunit in the double degron strain are reduced ~90%, but it is possible that low levels of intact SAGA contribute to genome-wide transcription. However, results from the Spt3/Taf13 and Spt7/Taf13 double degron strains strongly suggests that depletion of only one SAGA subunit is sufficient to

inactivate SAGA function (**Fig 2B**). This result shows that the weak effects of the SAGA degrons in otherwise WT cells is due to substantial redundancy with TFIID function at the coactivator-redundant genes rather than incomplete depletion.

Differences between "coactivator-redundant" genes and "SAGA-dominated" genes

Our TFIID-dependent and coactivator-redundant gene sets overlap with the categories previously defined: "TFIID-dominated" and "SAGA-dominated" (Huisinga and Pugh, 2004), however, there are significant differences. Our coactivator-redundant genes (655 genes) contain 2/3 of the SAGA-dominated gene set (273 genes) plus an additional 311 genes that were originally characterized as TFIID-dominated (**Fig S6A**). Therefore, our coactivator-redundant gene set is over 50% different from the SAGA-dominated gene set. There are corresponding differences in our TFIID-dependent vs the TFIID-dominated gene set. We suspect that these differences are mainly due to technical issues such as measurement of newly-synthesized vs steady state mRNA and the greater sensitivity and depth of the 4-thioU RNA-seq data compared with the microarray data used in the original analysis. These new results differ from our prior Pol II ChIP experiments that did not detect gene specific Taf requirements (Warfield et al., 2017). However, it was recently suggested that this may be due to background issues with Pol II ChIP data (e.g., stalled or paused Pols) and that Pol II ChIP is best used for quantitation of changes in highly expressed genes (Petrenko et al., 2019). This explanation is consistent with our new findings.

Importantly, our reclassification of many genes affects the interpretation of published studies examining coactivator function and specificity that relied on the SAGA-dominated and TFIID-dominated gene lists. For example, our prior collaborative study measured gene expression defects upon rapid depletion of SAGA subunit Spt7 by anchor away (Baptista et al., 2017). These results showed that expression of genes in both the SAGA-dominated and TFIID-dominated gene categories are sensitive to rapid SAGA inactivation, in apparent contrast to the above results. However, comparing the specific genes tested in this earlier work with our revised gene categories shows that 4/6 of the TFIID-dominated genes assayed by Spt7 anchor

away are in fact in the new coactivator-redundant gene class and are expected to be sensitive to rapid SAGA depletion. Therefore, the Spt7 anchor away results from the earlier study are largely consistent with our current findings.

Features of the TFIID-dependent and coactivator-redundant gene classes

When genes are sorted by transcription levels, determined by the amount of 4-thioU incorporated in 5 min, the ratio of coactivator-redundant to TFIID-dependent genes is relatively similar across the range of transcribed genes except for the most highly expressed, where the coactivator-redundant class is enriched (**Fig 3A, Fig S5B**). The bottom four expression quintiles have a relatively constant ratio of ~10%, but the fraction of genes in the coactivator-redundant category increases to ~30% in the top quintile and ~44% in the top 10% of expressed genes. The fraction of these genes increases even more dramatically when examining only the most highly expressed genes. Yeast Pol II transcription is dominated by a small number of very highly transcribed genes: the top 2% of expressed genes accounts for ~22% of total transcription (**Fig 3B; Fig S6B; Tables S1 and S2**). As an example of the coactivator bias in these exceptional genes, 47 of the top 50 expressed genes (94%; expression >195 in Fig 3B), are in the coactivator-redundant category (**Table S3**).

Since highly expressed genes are enriched for the coactivator-redundant class, we asked whether the sensitivity of individual genes in this set to rapid TFIID or SAGA depletion varies with expression. For example, are highly expressed genes more sensitive to rapid SAGA or TFIID depletion? **Fig 3C** shows a plot of the difference in sensitivity to rapid Taf13 or Spt3/7 depletion vs gene expression rank. From this plot, it is apparent that most of the coactivator-redundant genes (68%) are more sensitive to Taf13-depletion compared with rapid SAGA depletion (mean difference -0.49). This difference changes slightly when considering only the top 100 expressed genes that are equally divided between stronger TFIID and stronger SAGA-dependence (mean difference -0.07). Combined, our analysis shows that the relative reliance of the coactivator-redundant genes on either TFIID or SAGA is not a barrier to very high levels of transcription.

It was previously noted that the “SAGA-dominated” genes are enriched for TATA-containing promoters (Huisinga and Pugh, 2004), and the gene classes “SAGA-dominated” and “TATA-containing” are often equated in the literature (TATA was defined as TATAWAWR; (Basehoar et al., 2004). To investigate this, we used the list of TATA-like elements defined in (Rhee and Pugh, 2012) obtained from the YeasTSS database (www.yeastss.org), extracted the sequences of all annotated TATA-elements and reclassified promoters as TATA-containing/TATA-less based on the less stringent 7 nt consensus (TATAWAW). Although TATA-containing promoters are enriched, the coactivator-redundant class is clearly not equivalent to TATA-containing genes (**Fig 3D**). Our analysis shows that 60% of coactivator-redundant genes are classified as TATA-containing but that both the coactivator-redundant and TFIID-dependent gene sets contain a nearly equal number of TATA-containing genes using the above criteria.

To further investigate differences between the gene classes, we performed de novo motif discovery for sequences surrounding the TSS of genes in each class (-400 -> +100; Methods). This analysis found that the binding motifs for 14 transcription factors are preferentially enriched in one of the two gene classes (**Table S5**). For example, the binding motif for the general regulatory factor Reb1 is found near 18% of the TFIID-dependent genes vs 6% of all other genes while TATA, Msn2 and other motifs are preferentially enriched near the coactivator-redundant genes vs all other genes.

To examine these findings in more detail, we directly searched the set of genes used in our transcription analysis (~83% of all genes) for the Msn2/4 and TBP consensus binding motif (**Fig 3E, Table S5**; Methods). This search strategy doubled the number of genes identified as containing a TBP consensus binding site (TATAWAW) and many of these genes are in the TFIID-dependent category. However, the coactivator-redundant genes are clearly enriched for TATA (65% contain this motif) while the TATA motif is found in only ~1/4 of the TFIID-dependent genes. We also found that the Msn2/4 motif is enriched in the coactivator-redundant genes compared with the TFIID-dependent genes, although over three times the number of TFIID-dependent genes contain Msn2/4 motifs compared with coactivator-redundant genes (173 vs

609). Since no frequently used motif is found exclusively at either the TFIID or coactivator-redundant genes, our findings suggest that there is no one transcription factor or promoter sequence motif that determines whether a gene is in the coactivator-redundant or TFIID-dependent gene class.

The 136 ribosomal protein (RP) genes have sometimes been analyzed as a distinct category of highly expressed and especially TFIID-dependent genes. From analysis of our new data, we did not find that these genes are obviously distinct from many other genes based on TFIID or SAGA-dependence. Although 95% of the RP genes belong to the TFIID-dependent category they show comparable transcription defects upon TFIID depletion as the rest of the TFIID-dependent genes. However, RP genes are clearly more highly expressed than the average gene, with 83% of the RP genes found in expression quintile 5 (**Fig S7**). K-means clustering, based on TFIID and SAGA-dependence with up to 6 clusters, did not segregate the RP genes into a distinct category. Alternative methods we applied (hierarchical and spectral clustering) also did not separate RP genes into a distinct category. This analysis shows that RP genes have coactivator-dependence similar to many other genes. There can be good biological reasons to examine properties of RP genes as a separate category since they are regulated coordinately in response to several signaling pathways and this regulation is key for proper cellular growth and stress response. However, they do not seem exceptional in regard to TFIID and SAGA-dependence.

SAGA-dependent chromatin modifications change slowly after rapid SAGA depletion

We next investigated the basis for the difference in transcription phenotypes caused by the SAGA deletion vs degron strains. SAGA functions through direct protein-protein interactions to assist with TBP recruitment and PIC formation as well as via chromatin changes mediated by Gcn5 and Ubp8 (Bhaumik and Green, 2001; Dudley et al., 1999; Koutelou et al., 2010; Laprade et al., 2007; Larschan and Winston, 2001; Mohibullah and Hahn, 2008; Papai et al., 2019; Rodriguez-Navarro, 2009; Sermwittayawong and Tan, 2006). One possibility is that the modest transcription defects caused by rapid depletion are primarily mediated by disruption of TBP-

DNA loading and other non-enzymatic functions, while the stronger long-term effects of the *SPT* deletions are mediated in part through changes in chromatin modifications.

As an initial test of this model, we compared transcription levels in strains lacking specific SAGA-linked enzymatic functions *(gcn5Δ* or *ubp8Δ*), in an *spt3Δ* strain defective for SAGA TBP-binding function and, in cells after rapid SAGA-depletion (Spt3/7-degron) (**Fig 4**) (**Table S6**). We found that elimination of HAT function (*gcn5Δ*) led to a genome-wide transcription defect in both gene classes that was nearly as strong as that found in the *spt3Δ* mutant. Elimination of deubiquitination function (*ubp8Δ*) led to more modest genome-wide defects in transcription for both gene classes.

Since transcription defects in *SPT* deletion mutants are stronger than that caused by rapid SAGA depletion, we next examined the kinetics of changes in SAGA-dependent chromatin marks in the Spt-degron strains. The SAGA-dependent chromatin marks H3K18-Ac and H2B-Ub (Daniel et al., 2004; Henry et al., 2003; Morris et al., 2007) were monitored in the *SPT* deletion strains and after IAA addition to the Spt3/7 and Spt3/20 degron strains. Western blot analyses of whole cell extracts showed that the *spt3Δ*, *spt20Δ* and *spt7Δ* strains all had lower total levels of H3K18-Ac, ranging from ~34% of normal in the *spt7Δ* and *spt20Δ* strains to 70% of normal in the *spt3Δ* strain **(Fig 5A**, left panel; **Fig S8A**). H2B-Ub levels were also decreased in these mutants with values ranging from 16% - 29% of WT (**Fig 5A**, right panel; **Fig S8A**). As expected, higher levels of H2B-Ub are observed upon deletion of *UBP8*, encoding the H2B deubiquitinase. In contrast, upon activation of the Spt3/20 or Spt3/7 degrons, H3K18-Ac was >70% of WT levels after 30 min and thereafter decreased slowly over time (**Fig 5B**, left panel; **Fig S8A**). At 6 hrs after IAA addition to these strains, the levels of H3K18-Ac mark in bulk chromatin were reduced to 45-50% of WT. The levels of H2B-Ub did not show any consistent changes during this time course (**Fig 5B**, right panel). The weak H2B-Ub antibody reactivity likely contributes to the variable H2B-Ub signals.

To investigate changes in histone acetylation at individual promoters, we next examined changes in chromatin-associated H3K18-Ac marks using ChIP-seq (**Fig 5C, Fig S9A**) (**Table S7**). As expected, the bulk of this signal is associated with the +1 nucleosome (**Fig S9A**). We found a >10-fold average defect in promoter-linked H3 acetylation in the *gcn5Δ* and *spt7Δ* strains and a 3.3-fold defect in the *spt3Δ* strain. In contrast, after 30 min of SAGA depletion, we observed only a 1.7-fold reduction. These changes in H3 acetylation were nearly the same at both the TFIID-dependent and coactivator-redundant genes (**Fig S9B**), consistent with earlier findings that SAGA contributes to chromatin modifications at all expressed genes (Bonnet et al., 2014). As expected, little or no H3 acetylation change was observed in the *ubp8Δ* strain. Comparison of different experiments revealed very high consistency between results of *gcn5Δ*, *spt7Δ* and Spt3/7-degron experiments, while *spt3Δ* experiment showed a lower but still significant correlation (**Fig S9C**). Our combined results strongly suggest that defects in SAGA-regulated chromatin modifications, particularly defects in Gcn5-dependent H3 acetylation, are a major contributor to the genome-wide decrease in transcription observed at nearly all genes in the *SPT* deletion strains. Since these chromatin modifications change relatively slowly after rapid SAGA depletion, we propose that transcription changes caused by rapid SAGA depletion are primarily due to disrupting one or more direct roles of SAGA in promoting transcription such as TBP-DNA loading.

TFIID and SAGA map to both TFIID-dependent and coactivator-redundant genes

As discussed above, there has been disagreement in prior work as to the location and amount of TFIID binding to different gene classes. Early formaldehyde-based crosslinking studies showed that Tafs are generally depleted at the "SAGA-dominated" genes compared with the "TFIID-dominated genes", while MNase-based ChEC showed similar binding to both gene classes. We revisited this question using our revised gene lists and an improved ChEC-seq method that includes higher stringency criteria to map the genome-wide binding of these two coactivators. To minimize non-specific MNase cleavage and to avoid over digestion at authentic binding sites, we modified the original ChEC MNase cleavage conditions, using 10-fold lower calcium concentrations, and limited the MNase digestion time to 5 min. All experiments use

spike-in DNA to normalize the control and experimental samples for quantitation. ChEC DNA cleavage patterns are compared with MNase controls, generated from cells where free MNase with a nuclear import signal is expressed from a promoter with greater or equal activity as the factor under study. Detailed methods and the criteria for peak calling are described in Methods.

Using our updated ChEC-seq method to map Taf1, Taf7 and Taf13 binding (four biological replicates each), we identified 2938, 3681 and 3723 bound mRNA promoters, with extensive overlap between binding sites mapped with different Taf-MNase fusions (**Fig S10A**) (**Table S8**). Promoters were considered bound if a promoter-associated peak was called in at least 3 of 4 replicates. **Fig 6A** shows average plots of Taf-ChEC and control signals at the bound promoters and representative gene browser tracks are shown in **Fig S10B**. Using the above computational criteria, ~75% of TFIID binding sites identified by ChIP-exo (Vinayachandran et al., 2018) overlap with the sites identified by Taf1-MNase, showing a close correspondence in results between our updated ChEC-seq approach and ChIP-exo (**Fig S10C**).

We next used ChEC-seq to revisit genome-wide binding of SAGA, where Spt3-MNase and Spt7-MNase identified 1601 and 3536 promoter binding sites (**Fig S10A, B**) (**Table S8**). **Fig 6A** shows average plots of DNA cleavage from the Spt-MNase fusions and from free MNase. Our analysis showed that ~97% of SAGA binding sites mapped using Spt3-MNase overlap with the more extensive set of promoters mapped using Spt7-MNase (**Fig S10A**). Since Spt3 and Spt7 are thought to exist only in SAGA, the larger number of binding sites observed with Spt7-MNase likely indicates greater DNA accessibility of the MNase fusion.

Importantly, we found widespread promoter binding and ≥86% overlap in genes bound by TFIID and SAGA when comparing ChEC signals from Taf7 and Spt7-MNase fusions, supporting our findings above that most genes are regulated by both factors (**Fig 6B**). Further analysis showed little or no preference for the binding of TFIID or SAGA to either promoter class (**Fig 6C**). Taf13, Taf7, Taf1, and Spt7 MNase fusions all gave similar ratios of binding to each promoter type. The exception is the Spt3-MNase fusion that detected binding at fewer TFIID-dependent promoters

compared with the other MNase fusions. However, since Spt3 is not known to be in any complex other than SAGA, we think it likely that this difference is due to different DNA accessibility and/or the architecture of SAGA and other factors at the two promoter types. Taken together, the widespread mapping of TFIID and SAGA at both promoter types is consistent with SAGA and TFIID acting at nearly all genes.

Rapid SAGA depletion primarily affects maintenance of ongoing transcription rather than gene activation by Gcn4

Prior work showed that SAGA subunit deletion strains are defective in transcription activation at some genes (Bhaumik and Green, 2001; Dudley et al., 1999; Mohibullah and Hahn, 2008). To extend this work, we asked whether rapid SAGA depletion led to defects in activation of transcription (defined here as an increase in transcription in response to a stress signal) and/or in the maintenance of already ongoing transcription. Strains were grown in synthetic glucose media and RNA labeled for 5 min with 4-thioU followed by RT qPCR analysis of newly-synthesized mRNA. Transcription was first measured in either the *spt3Δ* or *spt7Δ* strains before or after addition of sulfometuron methyl (SM), which induces amino acid starvation and induction of Gcn4-dependent genes (**Fig 7A**). Transcription was measured at three TFIID-dependent genes (*ACT1, RPS5, SSH1*) that are not Gcn4 targets and three coactivator-redundant genes that are direct Gcn4 targets (*ARG3, HIS4, ARG5*). Compared with a wild type strain, the *SPT* deletion strains had ~3-fold lower expression levels at all three TFIID-dependent genes (compare light blue bars to light grey and light orange bars in **Fig 7A**). As expected, In the *SPT* deletion strains, these genes showed little or no transcription increase upon SM addition. At the three Gcn4 target genes, uninduced transcription was decreased >4-fold compared with WT and the response to SM was dependent on the *SPT* deletion. In the WT strain, activation of *ARG3*, *HIS4*, and *ARG5* ranges from 2.6 to 3.8-fold (**Fig 7A**, compare light and dark blue bars). Although the levels of both uninduced and activated transcription were reduced in the *spt7Δ* strain, the three Gcn4-dependent genes showed some activation (1.7 to 2.5-fold; light vs dark grey bars), while activation was eliminated in the *spt3Δ* strain (light vs dark orange bars).

To determine the consequence of rapid SAGA depletion before transcription was induced, cells containing the Spt3/7 double degrons were first treated with IAA for 30 min to deplete these proteins and then induced with SM for 60 min. This treatment still allowed for greater than normal fold-activation upon subsequent SM addition (3.6 to 6.9-fold; **Fig 7B;** light vs dark orange bars). In contrast, IAA added to already SM-induced cells reduced Gcn4-dependent transcription between 1.7 and 2.6-fold (light vs dark grey bars). Combined, our results show that, for Gcn4-dependent gene activation, the gene-specific role of SAGA is most important for efficiency or maintenance of ongoing transcription rather than for induction of transcription in response to an activation signal.

Discussion

Here we have investigated the genome-wide and gene-specific roles for the coactivators SAGA and TFIID. Several prior studies suggested that, while TFIID and SAGA make genome-wide contributions, transcription at nearly all genes is dominated by one or the other factor and that many highly expressed genes show only modest TFIID-dependence (Huisinga and Pugh, 2004; Petrenko et al., 2019). This view seemingly conflicts with other studies where TFIID and SAGA were found to have major genome-wide roles at most genes (Baptista et al., 2017; Bonnet et al., 2014; Warfield et al., 2017). Our new results bring together many of these findings and provide a new mechanistic explanation for many genes that showed significant Taf-independent expression in earlier studies: TFIID and SAGA function is substantially redundant at these genes, with WT expression levels promoted by both coactivators.

The expression of 4900 genes were analyzed for coactivator dependence (83% of all yeast protein coding genes that met our expression and reproducibility threshold). Rapid subunit depletion revealed two classes of genes with different dependencies on TFIID and SAGA. The first class, termed TFIID-dependent genes, contains 87% of the analyzed genes and shows strong transcription dependence on TFIID but little or no change in response to rapid depletion of SAGA. The second class, termed coactivator-redundant genes, contains 13% of analyzed genes and shows a modest transcription decrease in response to rapid depletion of either TFIID

or SAGA. Importantly, simultaneous depletion of both TFIID and SAGA leads to a severe transcription defect at these coactivator-redundant genes. This latter result is consistent with prior general conclusions that the combination of a SAGA subunit deletion and TFIID ts mutation can result in greater transcription defects compared with either single mutation (Huisinga and Pugh, 2004; Lee et al., 2000). Together, our results demonstrate that TFIID and SAGA have partially redundant function at the coactivator-redundant genes and, as described more fully below, we envision that these genes can use either the TFIID or SAGA pathways to promote TBP binding (**Fig 8**).

We also found that expression of nearly all genes is dependent on another SAGA function that was revealed in cells that had grown many generations without SAGA. Our results link this genome-wide role to SAGA-regulated chromatin modifications - marks that are slow to change upon rapid SAGA subunit depletion. Deletions in either *GCN5* or *UBP8,* the SAGA subunits responsible for chromatin modifications, show genome-wide transcription defects that are much stronger than those caused upon rapid SAGA depletion.

Western analysis of total chromatin showed that the level of H3K18-Ac and H2B-Ub are reduced in the *SPT* deletion strains and change slowly upon SAGA subunit depletion. Importantly, ChIP-seq analysis found that the levels of promoter-localized H3K18-Ac was much lower in the *SPT* deletion strains compared to strains depleted of SAGA function for 30 min. Indirect effects, such as decreased expression of general regulatory factors and components of the basal Pol II machinery, etc., likely also contribute to lower genome-wide expression in the deletion strains. The two roles of SAGA seem additive, which readily explains why the coactivator-redundant genes are more sensitive to *SPT* deletions compared to the TFIID-dependent genes. Our findings show that the coactivator-redundant genes require both SAGA functions while the TFIID-dependent genes are primarily dependent only on the SAGA-mediated chromatin modifications.

Yeast cellular transcription is dominated by a small number of exceptionally highly expressed genes and it was proposed that highly expressed genes are biased for Taf-independent expression (Petrenko et al., 2019). We do find that the coactivator-redundant genes, while spread throughout the range of expressed genes, are enriched in the top 10% of transcribed genes. However, analysis of the ratio of SAGA-dependence/Taf-dependence shows that, within this entire gene class, there is no obvious relationship between coactivator sensitivity and gene expression. In fact, this analysis shows that most genes in the coactivator-redundant gene class show more reliance on TFIID compared with SAGA.

Results from mapping the genome-wide locations of TFIID using an improved and more stringent ChEC-seq method are consistent with our findings that TFIID functions at both the TFIID-dependent and coactivator-redundant genes. We observe no bias in promoter type bound by either TFIID or SAGA. In contrast, prior studies have observed a bias in Taf-promoter binding using formaldehyde crosslinking. At this time, the reason for this discrepancy is unknown, although we previously speculated that the observed bias in proximity of TFIID to nucleosomes at TFIID-dependent genes (Rhee and Pugh, 2012) may play a role in Taf-DNA crosslinking efficiency (Warfield et al., 2017).

To examine features leading to the different coactivator responses, we conducted a *de novo* motif search of promoters in each class. As expected, the TATA consensus sequence is enriched in the coactivator-redundant class, although nearly equal numbers of TATA-containing genes are found in the TFIID-dependent gene set. The results of *de novo* search found 14 transcription factor motifs that are enriched in one or the other gene class. However, this and more directed searches for these consensus motifs showed that no transcription factor binding site is exclusive for one or the other gene class. For example, while the motif for the Msn2/Msn4 factors is enriched in the CR gene class compared with all other genes, the majority of Msn2/Msn4 binding motifs are found in TFIID-dependent genes. From this combined analysis, we conclude that the distinction between the gene classes is due to multiple components rather than any one factor or promoter sequence. These factors likely include the

specific regulatory transcription factors used at each promoter, promoter sequence and perhaps chromatin architecture.

From the above results, it is clear that the coactivator-redundant genes are dependent on both coactivators rather than their expression being dominated by SAGA as proposed earlier; when one coactivator is eliminated, the other can at least partially compensate. What is the mechanistic basis for this behavior? Both factors were shown to have TBP-DNA loading activity. Based on earlier studies, we propose that the TFIID-dependent genes exclusively require Tafs for promoter recognition and TBP-DNA loading while the coactivator-redundant genes can use either SAGA or TFIID. Since many CR genes contain TATA elements, we envision that SAGA can recruit TBP more directly, taking advantage of: (1) specific TBP-TATA interactions and (2) direct TBP interactions with other TBP-compatible DNA binding motifs. This model can explain the surprising viability of strains with TBP mutations that are defective in TATA-DNA binding (Kamenova et al., 2014). Some of these TBP mutants may be defective in the SAGA-mediated TBP loading pathway but still function in the TFIID-dependent pathway. We note that these two gene categories do not perfectly correlate with the presence or absence of TATA. It has been shown, however, that the TATA consensus sequence does not perfectly correlate with function and that sequences surrounding TATA are also important (Donczew and Hahn, 2018; Sprouse et al., 2008).

Finally, we found that rapid depletion of SAGA, primarily decreases ongoing and already activated transcription at several coactivator-redundant genes. In contrast, rapid depletion does not affect activation per se at three Gcn4-dependent genes. This result is surprising, since it was shown earlier that *SPT* deletion strains have defects in gene activation (Bhaumik and Green, 2001; Dudley et al., 1999). However, we now know that these strains are defective in both functions of SAGA, unlike in our rapid depletion experiments. Gene activation (defined here as an increase in transcription in response to a stress signal) requires a rapid increase in the recruitment of TBP and other PIC components. This activation process seems intact after rapid SAGA depletion, based on the ~2-fold increased ratios of induced/uninduced transcription

of Gcn4-dependent genes after SAGA depletion. It is important to note that, even though transcription is still inducible by Gcn4 after SAGA depletion, the absolute levels of basal and activated transcription are lower in these strains. We propose that these lower levels of basal and activated transcription explain why TFIID (without SAGA) can promote strong gene induction, while higher absolute levels of activated transcription in WT cells requires both coactivators.

From the available data, it is not yet clear why the coactivator-redundant genes require both SAGA and TFIID for efficient transcription. With the exception of the top 50 expressed genes, there are many genes in the top expression quintile that are TFIID-dependent and SAGA-independent. Therefore, the TFIID-directed pathway does not seem inherently limiting for relatively high transcription levels. Ongoing transcription, especially at very highly expressed genes, likely involves efficient transcription reinitiation via bursts of transcription. Efficient TBP-DNA loading may be important for this process at the coactivator-redundant genes and it will be of interest in future studies to probe these genes for defects in initiation, reinitiation and other steps in the transcription pathway after SAGA depletion.

Materials and methods

Strain Construction

S. cerevisiae strains (**Table S9**) were constructed using standard yeast methods. Proteins were chromosomally tagged by high efficiency yeast transformation and homologous recombination of PCR-amplified DNA. Plasmid pFA6a-3V5-IAA7-KanMX6 (Chan et al., 2018) was used as the template for generating the IAA7 degron tags. This C-terminal tag contains three copies of the V5 epitope tag followed by the IAA7 degron (32 kDa total). For ChEC-seq experiments proteins were tagged with 3xFLAG-MNase::TRP1MX6 using pGZ110 (Zentner et al., 2015). A strain expressing free MNase under control of the native *BDF1* promoter was constructed the following way. First, the *MED8* promoter in pSG79 (Grünberg et al., 2016) was exchanged with the *BDF1* promoter (containing 500 bp upstream DNA from the *BDF1* start codon). A XhoI/SacI fragment containing the P_{BDF1}-MNase fragment was inserted to the yeast integrating vector pRS303. The resulting pRD16 plasmid was linearized with BstEII and integrated into strain BY4705.

Yeast Cell Growth

S. cerevisiae strains were grown as indicated in either rich media (YPD: 1% yeast extract, 2% peptone, 2% glucose, 20 μg/ml adenine sulfate) or synthetic complete (SC) media (per liter: 1.7 g yeast nitrogen base without ammonium sulfate or amino acids (BD Difco), 5 g ammonium sulfate, 40 μg/ml adenine sulfate, 0.6 g amino acid dropout mix (without -Ile -Val) and supplemented with 2 micrograms/ml uracil and 0.01% other amino acids to complement auxotrophic markers). Standard amino acid dropout mix contains 2 g each of Tyr, Ser, Val, Ile, Phe, Asp, Pro and 4 g each of Arg and Thr. *S. pombe* strains were grown in YE media (0.5% yeast extract, 3% glucose). Where indicated, *S. cerevisiae* strains at an A600 of ~ 1.0 were treated with 500 μM indole-3-acetic acid (IAA) dissolved in DMSO (or with DMSO alone) for 30 minutes. Where indicated, cells were incubated with 0.5 μg/ml sulfometuron methyl (SM) in DMSO (SM) or with DMSO alone for 60 minutes as described in the text and figure legends, prior to RNA labeling.

Western Blot Analysis

1 ml cell culture was collected and pelleted from strains after treatment with IAA or DMSO, washed with 500 µl water, then resuspended in 75 µl yeast whole cell extract buffer. After heating for 5 min at 95°C, samples were centrifuged for 5 min at max speed, whole cell extracts were separated by SDS-PAGE and analyzed by Western blot using mouse monoclonal or rabbit polyclonal antibodies. To efficiently visualize histone marks, 5-10 ml of cell culture (adjusted to similar cell count based on OD measurement) was transferred to a tube on ice containing 2 ml 50 mM Tris, pH 7.5 + 10 mM NaN_3. Cells were pelleted, then resuspended in 75 ul SUTEB lysis buffer (10 mM Tris-HCl, pH 8.0, 1% SDS, 8M Urea, 10 mM EDTA, pH 8.0, 0.01% bromophenol blue) and transferred to a microcentrifuge tube, heated to 100°C for 4 min, then an equal volume of 0.5 mm zirconia/silica beads was added. Cells were lysed in a Mini Beadbeater-96 (BioSpec Products) for 30 sec followed by 1 min rest on ice and repeated for a total of four cycles. 200 ul additional SUTEB lysis buffer was added, vortexed, and extracts were heated to 100°C for 1 min. Extracts were transferred to new tubes and stored at -70°C until separated by SDS-PAGE. Protein signals were visualized by using the Odyssey CLx scanner and quantified using Odyssey Image Studio software (Li-Cor) by generating a standard curve using a titration from WT extract. Each protein analyzed was normalized to the amount of the TFIIF subunit Tfg2. H2B-Ub was probed with antibody 5546 (Cell Signaling Technology) and H3K18-Ac with antibody 07-354 (EMD Millipore).

RNA Labeling and mRNA purification for RT-qPCR

Newly synthesized RNAs were labeled as previously described (Bonnet et al., 2014). 10 ml *S. cerevisiae* or 20 ml *S. pombe* cells were labeled with 5 mM 4-thiouracil (Sigma-Aldrich) for 5 minutes, the cells were pelleted at 3000 x g for 2 minutes, flash-frozen in liquid N_2, and then stored at -80°C until further use. *S. cerevisiae* and *S. pombe* cells were mixed in an 8:1 ratio and total RNA was extracted using the RiboPure yeast kit (Ambion, Life Technologies) using the following volumes: 480 µl lysis buffer, 48 µl 10% SDS, 480 µl phenol:$CHCl_3$:isoamyl alcohol (25:24:1) per *S. cerevisiae* pellet + 50 µl *S. pombe* (from a single *S. pombe* pellet resuspended in 850 µl lysis buffer). Cells were lysed using 1.25 ml zirconia/silica beads in a Mini Beadbeater-96

(BioSpec Products) for 3 min followed by 1 min rest on ice. This bead beading cycle was repeated twice for a total of 3 times. Lysates were spun for 5 min at 16K x g, then the following volumes combined in a 5 ml tube: 400 µl supernatant, 1400 µl binding buffer, 940 µl 100% ethanol. Samples were processed through the Ambion filter cartridges until all sample was loaded, then washed with 700 µl Wash Solution 1, and twice with 500 µl Wash Solution 2/3. After a final spin to remove residual ethanol, RNA was eluted with 25 µl 95°C preheated Elution Solution. The elution step was repeated, and eluates combined. RNA was then treated with DNaseI using 6 µl DNaseI buffer and 4 µl DNaseI for 30 min at 37°C, then treated with Inactivation Reagent for 5 min at RT. RNA was then biotinylated essentially as described (Duffy et al., 2015; Duffy and Simon, 2016) using 40 µl (~40 µg) total RNA and 4 µg MTSEA biotin-XX (Biotium) in the following reaction: 40 µl total 4-thioU-labeled RNA, 20 mM HEPES, 1 mM EDTA, 4 µg MTSEA biotin-XX (80 µl 50 µg/ml diluted stock) in a 400 µl final volume. Biotinylation reactions occurred for 30 min at RT with rotation and under foil. Unreacted MTS-biotin was removed by phenol/$CHCl_3$/isoamyl alcohol extraction. RNA was precipitated with isopropanol and resuspended in 100 µl nuclease-free H_2O. Biotinylated RNA was purified also as described (Duffy and Simon, 2016) using 80 µl MyOne Streptavidin C1 Dynabeads (Invitrogen) + 100 µl biotinylated RNA for 15 min at RT with rotation and under foil. Prior to use, MyOne Streptavidin beads were washed in a single batch with 3 X 3 ml H_2O, 3 X 3 ml High Salt Wash Buffer (100 mM Tris, 7.4, 10 mM EDTA, 1 M NaCl, 0.05% Tween-20), blocked in 4 ml High Salt Wash Buffer containing 40 ng/µl glycogen for 1 hour at RT, then resuspended to the original volume in High Salt Wash Buffer. After incubation with biotinylated RNA, the beads were washed 3 X 0.8 ml High Salt Wash Buffer, then eluted into 25 µl streptavidin elution buffer (100 mM DTT, 20 mM HEPES 7.4, 1 mM EDTA, 100 mM NaCl, 0.05% Tween-20) at RT with shaking, then the elution step repeated and combined for a total of 50 µl. At this point, 10% input RNA (4 µl) was diluted into 50 µl streptavidin elution buffer and processed the same as the labeled RNA samples to determine the extent of recovery. 50 µl each input and purified RNA was adjusted to 100 µl with nuclease-free water and purified on RNeasy columns (Qiagen) using the modified protocol as described (Duffy and Simon, 2016). To each 100 µl sample, 350 µl RLT lysis buffer (supplied by the Qiagen kit and supplemented with 10 µl 1% βME per 1 ml RLT) and 250 µl 100% ethanol

was added, mixed well, and applied to columns. Columns were washed with 500 µl RPE wash buffer (supplied by the Qiagen kit and supplemented 35 µl 1% βME per 500 µl RPE), followed by a final 5 min spin at max speed. RNAs were eluted into 14 µl nuclease-free water.

After purification of mRNA, one sample per batch of preps prepared in a single day was tested for enrichment of labeled RNA by RT qPCR, probing both unlabeled and labeled RNA from at least 3 transcribed genes. The purified 4TU RNA typically contained 2-10% contamination of unlabeled RNA. We also analyzed the RNA-seq data for enrichment of intron-containing RNA in the purified 4TU-labeled samples (**Fig S3B**). As expected, intron-containing RNA is clearly enriched in the newly synthesized RNA compared with total RNA.

cDNA Synthesis and Quantitative PCR of newly-synthesized RNA

Two microliters RNA was used to generate cDNA using Transcriptor (Roche), random hexamer primer, and the manufacturer's instructions. cDNA was used either undiluted, 1/20, or 1/100 for quantitative PCR (qPCR) depending on the gene analyzed. Gene-specific qPCR was performed in triplicate using primers near the 5' end of the gene. qPCRs were assembled in 5 µl reaction mixtures in a 384-well plate using 2X Power SYBR green master mix (Thermo Fisher Scientific) and reactions were run on the QuantStudio5 Real-Time System (Thermo Fisher Scientific). Relative amounts of DNA were calculated using a standard curve generated from 10-fold serial dilutions of purified genomic DNA ranging from 10 ng to 0.001 ng. Relative amounts of *S. cerevisiae* transcript were normalized to *S. pombe* tubulin transcripts. All values are expressed relative to that of either wild type +SM or the Spt3/7-deg +SM strain, which were set to 1.0. Each experiment was performed in two biological replicates (cultures collected on separate days) and three technical replicates (independent measurements of the same qPCR sample). Values for technical replicates were averaged which gave a single value for each biological replicate. The final result is a mean of biological replicates.

Preparation of 4ThioU RNA Libraries for NGS

Newly synthesized RNA isolated via 4-thioU labeling and purification was prepared for sequencing using the Ovation SoLo or Ovation Universal RNA-seq System kits (Tecan) according to the manufacturer's instructions and 1 ng (SoLo) or 50 ng (Universal) input RNA. Libraries were sequenced on the Illumina HiSeq2500 platform using 25 bp paired-ends at the Fred Hutchinson Genomics Shared Resources facility.

ChEC-seq experiments

ChEC-seq was performed as previously described (Grünberg et al., 2016; Zentner et al., 2015) with several modifications. The final calcium concentration in the reaction mixture was 0.2 mM (2 mM in the original protocol) and MNase digestion was done for 5 min for all collected samples. Stop buffer was supplemented with *D. melanogaster* MNase-digested DNA (1 ng/ml stock concentration) in the amount calculated based on *S. cerevisiae* culture A600 measurement (volume = A600 x 8 μl).

ChIP-seq experiments

ChIP-seq was performed similarly as described (Rodriguez et al., 2014) with the following modifications. Zirconia/silica beads were used for bead beating. Chromatin was sonicated for three rounds of 15 min. *S. pombe* (strain 972h) chromatin used as a spike-in was prepared the same way as *S. cerevisiae* samples (including cross linking, bead beating and sonication) and supplied by the Tsukiyama lab (Fred Hutch). Each IP reaction contained 1 μg of *S. cerevisiae* chromatin, 10 ng of *S. pombe* chromatin and 20 μl of Protein G Dynabeads (Invitrogen, #10004D) conjugated with 4 μl of anti-H3K18-Ac antibody (EMD Milipore, #07-354) and the final volume was brought to 500 μl with FA buffer. 25 μl of the *S. cerevisiae*/*S. pombe* chromatin mix was transferred to a separate tube as an 'input' sample before addition of beads and combined with 25 μl of the stop buffer. Chromatin-antibody complexes were eluted with two 25 μl volumes of stop buffer. IP and input samples were processed together from this point. After Proteinase K digestion, DNA was purified by phenol extraction (two step extraction for input samples) followed by ethanol precipitation in the presence of 20 μg glycogen. Pelleted DNA was washed with 70% ethanol and resuspended in 15 μl 10 mM Tris-HCl (pH 7.5).

Preparation of sequencing libraries for ChEC-seq and ChIP-seq samples

Sequencing libraries were prepared similarly as described (Warfield et al., 2017) with several modifications. 1/6 vol of the final ChEC DNA sample and 2 ng of ChIP samples were used as an input. Final adapter concentration during ligation was 6.5 nM. Following ligation, in case of ChEC-seq samples two-step cleanup was performed using 0.25X vol AMPure XP reagent in the first step and 1.1X vol in the second step. 18 cycles were used for library amplification for ChEC-seq samples and 15 cycles for ChIP-samples. All libraries were sequenced on the Illumina HiSeq2500 platform using 25 bp paired-ends at the Fred Hutchinson Cancer Research Center Genomics Shared Resources facility.

Analysis of DNA sequencing data

The majority of the data analysis tasks except sequence alignment, read counting and peak calling (described below) was performed through interactive work in the Jupyter Notebook (https://jupyter.org) using Python programming language (https://www.python.org) and short Bash scripts. All figures were generated using Matplotlib and Seaborn libraries for Python; (https://matplotlib.org; https://seaborn.pydata.org). All code snippets and whole notebooks are available upon request.

Paired-end sequencing reads were aligned to *S. cerevisiae* reference genome (sacCer3) and *S. pombe* reference genome (ASM294v2.20) with Bowtie2 (Langmead and Salzberg, 2012) using optional arguments "-I 10 -X 700 --local --very-sensitive-local --no-unal --no-mixed --no-discordant". Details of the analysis pipeline depending on the experimental technique used are described below.

Analysis of RNA-Seq data

SAM files for *S. cerevisiae* data were used as an input for HTseq-count (Anders et al., 2015) with default settings. The GFF file with *S. cerevisiae* genomic features was downloaded from the Ensembl website (assembly R64-1-1). Signal per gene was normalized by the number of all *S.*

pombe reads mapped for the sample and multiplied by 10000 (arbitrarily chosen number). Genes classified as dubious, pseudogenes or transposable elements were excluded leaving 5797 genes for the downstream analysis. As a next filtering step, we excluded all the genes that had no measurable signal in at least one out of 48 samples including SAGA and TFIID degron experiments and *SPT3*, *SPT7* and *SPT20* deletion experiments (samples for simultaneous depletion of SAGA and TFIID, *GCN5* and *UBP8* deletion experiments and WT control auxin experiment were not used for this filtering step). The remaining 5158 genes were sorted by the average expression level based on combined results of all WT and DMSO samples (22 samples total). For this analysis, signal per gene was further normalized by the gene length. Results from all relevant samples were averaged and genes were ranked (**Table S1**). We used this information to filter out genes with the lowest expression after comparing average coefficient of variation for each sample at different cutoffs for the number of highly expressed genes left in the analysis. The biggest relative decrease in observed average CV was visible after filtering out 5% (258) lowly expressed genes. Consequently, 95% of 5158 genes (i.e. 4900 genes) were used in the rest of this work. The results of biological replicate experiments for each sample were averaged (**Table S2**). All experiments were done in triplicate except YPD Taf-degron and wild-type BY4705 samples (labeled SHY772) that were done in duplicate. Replicate experiments showed low variation for the majority of genes which is visualized in **Fig S1** using coefficient of variation. Data for simultaneous depletion of SAGA and TFIID, *GCN5* and *UBP8* deletion experiments and WT control auxin experiment was limited to the same set of 4900 highly expressed genes and the results of biological replicates (two or three) were averaged. Corresponding samples were compared to calculate $\log_2$ change in expression per gene (IAA to DMSO samples for degron experiments and deletion mutant to WT strain for SAGA deletion experiments – strain BY4705 (Brachmann et al., 1998) was used as a background for *SPT20*, *SPT7*, *GCN5* and *UBP8* deletion strains, SHY565 (BY4705 with Rpb3-3xFlag::KanMX) was used to construct the *SPT3* deletion strain) and degron strains are derivatives of SHY1037 (Warfield et al., 2017) (**Table S9**).

Analysis of ChEC-seq data

SAM files for *S. cerevisiae* data were converted to tag directories with the HOMER (http://homer.ucsd.edu, (Heinz et al., 2010) 'makeTagDirectory' tool. Peaks were called using HOMER 'findPeaks' tool with optional arguments set to '-o auto -C 0 -L 2 -F 2', with the free MNase data set used as a control. These settings use default false discovery rate (0.1%) and require peaks to be enriched 2-fold over the control and 2-fold over the local background. Resulting peak files were converted to BED files using 'pos2bed.pl' program. For each peak, the peak summit was calculated as a mid-range between peak borders. For peak assignment to promoters the list of all annotated ORF sequences (excluding sequences classified as 'dubious' or 'pseudogene') was downloaded from the SGD website (https://www.yeastgenome.org). The data for 5888 genes was merged with TSS positions obtained from (Park et al., 2014). If the TSS annotation was missing, the TSS was manually assigned at position -100 bp relative to the start codon. Peaks were assigned to promoters if their peak summit location was in the range from -300 to +100 bp relative to the TSS. In a few cases, where more than one peak was assigned to the particular promoter, the one closer to the TSS was used. The lists of bound promoters for replicate experiments were compared and only promoters bound in three out of four replicates were used in downstream analysis. In cases a promoter did not have a peak assigned in one of the replicates we used the position of the strongest signal around the TSS as the peak summit. Manual inspection of many of these cases confirmed the validity of this approach.

Coverage at each base pair of the *S. cerevisiae* genome was calculated as the number of reads that mapped at that position divided by the number of all *D. melanogaster* reads mapped in the sample and multiplied by 10000 (arbitrarily chosen number). Signal per promoter was calculated for each replicate experiment as a sum of normalized reads per base in a 300 bp window around the peak summit. The overall signal per promoter (**Table S8**) is the average signal from all replicate experiments.

FASTQ files for the Taf1 ChIP-exo were obtained from the SRA (SRR5511893) (Vinayachandran et al., 2018). The data was processed as described above except for the use of RPM normalization.

1

2 **Analysis of ChIP-seq data**

3 Coverage at each base pair of the *S. cerevisiae* genome was calculated as the number of reads
4 that mapped at that position divided by the number of all *S. pombe* reads mapped in the
5 sample, multiplied by the ratio of *S. pombe* to *S. cerevisiae* reads in the corresponding input
6 sample and multiplied by 10000 (arbitrarily chosen number). The list of all annotated ORF
7 sequences (excluding sequences classified as 'dubious' or 'pseudogene') was downloaded from
8 the SGD website (https://www.yeastgenome.org). The data for 5888 genes was merged with
9 TSS positions obtained from (Park et al., 2014). If the TSS annotation was missing the TSS was
10 manually assigned at position -100 bp relative to the start codon. H3K18-Ac signal per gene was
11 calculated for each replicate experiment as a sum of normalized reads per base in a window
12 between 200 bp upstream and 300 bp downstream from TSS. We excluded three genes which
13 had no measurable signal in at least one sample. The results of biological duplicate experiments
14 for each sample were averaged and the change in H3K18-Ac signal per gene was calculated by
15 comparing corresponding samples – IAA to DMSO samples for degron experiments and deletion
16 mutant to WT strain for SAGA deletion experiments. Strain BY4705 (Brachmann et al., 1998)
17 was used as a background for *SPT7, GCN5* and *UBP8* deletion strains, SHY565 (BY4705 with
18 Rpb3-3xFlag::KanMX) was used to construct the *SPT3* deletion strain. The final dataset contains
19 $\log_2$ change in H3K18-Ac signal values per gene for 5885 genes (**Table S7**).

20

21 **K-means clustering analysis**

22 K-means clustering was performed using 'KMeans' function from Python sklearn.cluster library
23 with default settings. Two clusters were found to give the best separation using silhouette
24 analysis ('silhouette-score' function from sklearn.cluster library). Log_2 change in transcription
25 values from all SAGA deletion experiments and all TFIID degron experiments were used and all
26 4900 genes which gave reproducible results in RNA-seq (as described above) were included in
27 the analysis.

28

29 ***De novo* motif discovery**

De novo motif discovery was performed using HOMER (http://homer.ucsd.edu) (Heinz et al., 2010) 'findMotifs.pl' program. Motif length was set to be in a range 6 – 16 bp and the promoter region was defined as the area between 400 bp upstream to 100 bp downstream from TSS. Promoters from the analyzed class were screened against all other yeast promoters. Resulting motifs were screened against the library of known motifs from HOMER database and the best matches were reported (**Table S5**). Two most highly represented motifs for CR genes (TATA box and Msn2/4 binding site) were chosen for more detailed analysis. Each of these two motifs was searched for among 4900 promoters classified in this study. For TATA box a consensus TATAWAW was used and the search was limited to the region from 200 bp upstream to TSS. For Msn2/4 a consensus (A/C/G)AGGGG was used (Stewart-Ornstein et al., 2013) and the search was limited to the region from 300 bp upstream to 50 bp upstream relative to TSS. All promoters carrying at least one consensus sequence in a defined range were classified as either TATA-containing or Msn2/4-containing.

Data availability

The data discussed in this publication have been deposited in NCBI's Gene Expression Omnibus and are accessible through GEO Series accession number GSE142122 (available after peer review).

Author contributions

LW, RD and DP performed all experiments, RD performed computational analysis of ChIP-seq and ChEC-seq data, RD and AE performed computational analysis of RNA-seq data, and RD, LW and SH designed the study, analyzed the data, and wrote the manuscript.

Acknowledgements

We thank Gabe Zentner and Steve Henikoff for discussions, Christine Cucinotta and Brian Strahl for advice on SAGA-regulated chromatin modifications and detection, Wei Sun for discussion regarding clustering approaches, Matthew Fitzgibbon for helpful comments about RNA-seq data analysis, Toshi Tsukiyama for *S. pombe* chromatin, Steve Henikoff for *D. melanogaster*

chromatin and Laszlo Tora, Didier Devys, and Toshi Tsukiyama for comments on the manuscript. Supported by NIH grants GM053451 and GM075114 to SH and NIH P30 CA015704 to the Fred Hutch Genomics and Computational Shared Resources facility.

Table and figure legends

Figure 1. Two distinct classes of yeast genes based on SAGA and TFIID dependence. (**A**) Scatter plots comparing normalized signal per gene in corresponding samples. Log_{10} scale is used for X and Y axes. Mean values from replicate experiments are plotted. All presented experiments were done in SC media. (**B**) Heatmap representation of log_2 change in transcription values. Mean values from replicate experiments are plotted. Genes are grouped by results of k-means clustering analysis of SAGA deletion and TFIID degron experiments. Two clusters were found to give the best separation using silhouette analysis. Log_2 change values from relevant experiments for all 4900 genes were used as an input for k-means algorithm ('KMeans' function from Python sklearn.cluster library with default settings).

Figure 2. Simultaneous depletion of SAGA and TFIID severely affects transcription from almost all genes. (**A**) Box plot showing the log_2 change in transcription per gene upon perturbing cellular levels of SAGA or TFIID. Genes are divided into two classes according to results of the k-means clustering analysis of SAGA deletion and TFIID degron experiments from Fig 1. Mean values from replicate experiments are plotted. (**B**) Box plot and (**C**) heat map comparing results of depletion of SAGA or TFIID with simultaneous depletion of both coactivators. Genes are grouped into two categories from Fig 1. All experiments in panels B and C were done in SC media. Mean values from replicate experiments are plotted.

Figure 3. Properties associated with TFIID-dependent and coactivator-redundant genes. (**A**) Bar plot comparing the number of genes in each gene class as a function of expression level (left panel) and among the top 10% highly transcribed genes (right panel). Quintile 5 contains the most highly expressed genes. (**B**) Scatter plot of average expression vs the gene expression rank. Gene with rank 1 is most highly expressed. (**C**) Scatter plot comparing gene expression rank with the difference in sensitivity of genes to rapid Taf13 and Spt3/7 depletion. Only coactivator-redundant (CR) genes are plotted (655 genes). (**D**) Number of TFIID and coactivator-redundant (CR) genes among TATA-less and TATA-containing categories. Consensus TATA was defined as TATAWAW and the TATA-element positions from Pugh and colleagues (Rhee and

Pugh, 2012) were used. (**E**) Results of a motif search guided by results of *de novo* motif discovery (Methods). TATA box and Msn2/4 binding site were the most highly represented motifs for CR genes (**Table S5**). Each motif was searched among all 4900 promoters classified in this study. For TATA box, a consensus TATAWAW was used and the search was limited to the area from 200 bp upstream to TSS. For Msn2/4 a consensus (A/C/G)AGGGG was used (Stewart-Ornstein et al., 2013) and the search was limited to a region from 300 bp upstream to 50 bp upstream relative to TSS. All promoters carrying at least one consensus sequence in the defined range were classified as containing either TATA or the Msn2/4 binding site.

Figure 4. Changes in transcription (from 4thioU RNA-seq) observed in the SAGA deletion strains and in the Spt3/7 degron strain after rapid depletion. Mean values from replicate experiments are plotted and the genes are divided into TFIID-dependent and coactivator-redundant (CR) categories.

Figure 5. Histone modifications in *SPT* deletion and degron strains. (**A, B**) Quantitation of total H3K18-Ac and H2B-Ub in the *SPT* deletion and degron strains, normalized to the TFIIH subunit Tfg2 as a loading control. Data is from Fig S8. In panel (B), time after IAA or DMSO addition is indicated. (**C**) Box plot showing the ChIP-seq assayed $\log_2$ change per gene in H3K18-Ac signal in the SAGA deletion mutants and Spt3/7 degron strain. Degron strain was treated for 30 min with IAA before formaldehyde crosslinking. Mean values from replicate experiments are plotted.

Figure 6. TFIID and SAGA show widespread binding to both gene classes. (**A**) Average plots of Taf1, Taf7, Taf13, Spt3 and Spt7 ChEC DNA cleavage versus free MNase cleavage. Signals were averaged for bound promoters only. (**B**) Venn diagram showing the overlap of bound promoters in Taf7 and Spt7 experiments. (**C**) Number of promoters bound by the indicated subunit of TFIID or SAGA with genes separated into coactivator-redundant and TFIID-dependent gene categories.

Figure 7. Rapid SAGA depletion does not prevent transcription activation by Gcn4. (**A**) RT-qPCR analysis of 4-thio Uracil labeled RNA purified from indicated *SPT* deletion strains in the presence or absence of SM or (**B**) from *SPT*-degron strains induced with SM either before or after treatment with IAA. Samples were normalized by spike-in of labeled *S. pombe* cells before RNA isolation, and RT qPCR values from each *S. cerevisiae* gene were normalized to the value of the *S. pombe* tubulin gene. Each experiment was performed in two biological and three technical replicates. Error bars represent the standard error of the mean for two biological replicates (values obtained after averaging results for three technical replicates).

Figure 8. Model for roles of TFIID and SAGA and two different gene classes. Of the ~83% of yeast protein-coding genes analyzed in this study (4900 genes), the number of genes in each class is shown. Expression of genes in the TFIID set is strongly TFIID-dependent with little or no change after rapid SAGA depletion. TFIID and SAGA both contribute to expression of the coactivator-redundant genes where these factors have substantial overlapping function as revealed by rapid depletion experiments. Prior work suggests that these effects are due in part to the TBP-promoter DNA loading functions of TFIID and SAGA. Expression of nearly all genes is dependent on a separate function of SAGA, revealed by deletions in SAGA subunit genes, that is strongly linked to chromatin modifications that change slowly after rapid SAGA depletion.

Figure S1. (related to Figs 1 and 2). (**A**) Average coefficients of variation (CV) for selected experiments vs the percentage of genes analyzed (after first filtering out 639 genes which did not have RNA-seq signal in at least one experiment and sorting the remaining 5158 genes by expression level). CV values were calculated for each gene based on normalized read counts. Genes were sorted by the expression level. The biggest relative decrease in observed average CV is visible after filtering out 5% lowly expressed genes. Consequently 95% of 5158 genes (i.e. 4900 genes) were used in the rest of this work. **(B**) Gene-specific coefficients of variation (CV) for all 4-thioU RNA-seq experiments. All samples were done in triplicate except the YPD-grown Taf-degron cultures and wild-type BY4705 samples (labeled SHY772) that were done in

duplicate. CV values were calculated for each gene based on normalized read counts for replicate experiments.

Figure S2. (related to Figs 1 and 2). (**A**) Degron depletion in single or double degron strains. Western blot showing degron efficiency in cells grown in synthetic complete media. Experiment was done in biological triplicates (A, B, and C cultures). Variable amounts of the untreated samples were loaded to allow quantitation of degron efficiency. Blots were probed with a-V5 monoclonal (Spt20, Spt3, Spt7, Taf13, Taf1, Taf7-degrons) or a-Tfg2 polyclonal antibodies. (**B**) Western analysis of TFIID subunits in Taf-degron strains grown in YPD. Experiment was done in biological duplicates (A and B cultures).

Figure S3. (**A**) Box plot of gene expression level in selected experiments following DMSO treatment. Mean value for replicate samples was used. Log_{10} scale is used for Y axis. (**B**) Genome browser images showing the comparison of signal at selected intron-containing genes between total RNA sample and 4TU RNA-enriched sample.

Figure S4. (**A**) Correlation matrix of Pearson correlation coefficient values between log_2 changes in transcription in SAGA and TFIID depletion experiments and the slow growth signature defined in (O'Duibhir et al., 2014). Mean values from replicate experiments were used. (**B**) Bar plot showing the viability of degron-containing and WT yeast after a 30 min incubation with IAA. Viability measured in duplicate cultures by growth on YPD plates lacking IAA. (**C)** Correlation matrix of Pearson correlation coefficient values between log_2 changes in transcription in all SAGA and TFIID depletion experiments. Mean values from replicate experiments were used.

Figure S5. (related to Fig 2) (**A**) Scatter plots comparing results of Taf13-deg and Taf13/Spt3-deg experiments for coactivator-redundant (CR) genes and TFIID genes. (**B**) Scatter plot of gene expression rank vs the difference between the results of Spt3/Taf13-degron experiment and

the sum of effects of independent depletions of SAGA and TFIID (Spt3/20-deg and Taf13-deg experiments). Only CR genes are plotted (655 genes). Gene with rank 1 is most highly expressed.

Figure S6. (related to Fig 3) Properties of the TFIID and coactivator-redundant gene classes. (**A**) Barplot comparing previously defined categories "TFIID-dominated" and "SAGA-dominated" genes (Huisinga and Pugh, 2004) with categories defined in this study. (**B**) Boxplot representation of average expression per gene in expression quintiles based on 4thioU RNA labeling.

Figure S7. (related to Fig 3) The number of ribosomal protein (RP) genes within each expression quintile.

Figure S8. (related to Fig 5) Histone modifications in *SPT* deletion and degron strains. (**A, B**) Quantitation of total H3K18-Ac and H2B-Ub in the *SPT* deletion and degron strains as indicated. Depletion of the degron-tagged subunits is also shown. Data used for quantitation in Fig 5. Variable amounts of wild-type samples without IAA treatment were loaded to allow quantitation of histone modifications. Blots were probed with α-H3K18-Ac, α-H2B-Ub, α-Tfg2, α-H3 polyclonal antibodies and α-V5 monoclonal antibodies (for the degron-tagged subunit) as indicated.

Figure S9. (related to Fig 5) ChIP-seq analysis of H3K18-Ac signal in the SAGA deletion mutants and Spt3/7 degron strains. The degron strain was treated for 30 min with IAA or DMSO before formaldehyde crosslinking. (**A**) Genome browser images showing comparison of normalized signal at representative genomic locations. Mean values from replicate experiments are shown. (**B**) Box plot showing the $\log_2$ change per gene in H3K18-Ac signal in the SAGA deletion mutants and Spt3/7 degron strain. Genes are divided into two classes according to results of the k-means clustering analysis of SAGA deletion and TFIID degron experiments from Fig 1. Mean values from replicate experiments are plotted. (**C**) Correlation matrix of Pearson correlation

coefficient values between log_2 changes in H3K18-Ac signal in the SAGA deletion mutants and Spt3/7 degron strain. Mean values from replicate experiments were used.

Figure S10. (related to Fig 6) (**A**) Venn diagrams showing the overlap of promoters bound by different factors. (**B**) Genome browser images showing comparison of normalized signal at representative genomic locations. Identified binding sites, found in at least three out of four replicate experiments are marked by red stars. (**C**) Venn diagram comparing promoters bound by Taf1 as assayed by ChEC-seq or ChIP-exo (Vinayachandran et al., 2018).

Figure S11. (related to Fig 7) Degron efficiency in synthetic complete media with or without SM induction and IAA addition. (**A**) Western analysis of the Spt/7-degron strain without SM and with or without IAA. (**B**) Western analysis of the Spt3/7-degron strain treated with SM either before or after IAA addition. Blot was probed with α-V5 antibody (degron-tagged proteins) and α-Tfg2 as control.

Table S1. (Related to Figure 1) Spike-in normalized signal for all genes (5158) which had detectable transcription in 48 RNA-seq samples collected in this study (samples for simultaneous depletion of SAGA and TFIID, *GCN5* and *UBP8* deletion experiments and WT control auxin experiment were not used for this analysis). Expression column is the average signal for all DMSO and WT samples. This value was further normalized by the gene length to give normalized expression which was used to sort the genes from the highest to the lowest expression.

Table S2. (Related to Figure 1) Average spike-in normalized signal for replicate experiments for the final set of 4900 genes analyzed in this study and average expression per gene (based on DMSO and WT experiments). Rows are sorted by the average expression.

Table S3. (Related to Figures 1 and 2) Average $\log_2$ changes in transcription in the degron and deletion strains, results of k-means clustering and average expression per gene (based on DMSO and WT experiments). Rows are sorted by the average expression.

Table S4. (Related to Figure 2) Average $\log_2$ changes in transcription from degron experiments simultaneously depleting SAGA and TFIID components (Spt3/Taf13 and Spt7/Taf13). Data for other strains, results of k-means clustering and average expression per gene are the same as shown in table S3. Rows are sorted by the average expression.

Table S5. (Related to Figure 3) Motif enrichments found in the TFIID-dependent and coactivator-redundant gene classes.

Table S6. (Related to Figure 4) Average $\log_2$ changes in transcription for *GCN5* and *UBP8* deletion experiments. Data for other strains, results of k-means clustering and average expression per gene are the same as shown in table S3. Rows are sorted by the average expression.

Table S7. (Related to Figure 5) Average $\log_2$ changes in H3K18-Ac signal in the SAGA deletion mutants and Spt3/7 degron strain.

Table S8. (Related to Figure 6) Average spike-in normalized ChEC signals at bound promoters for the following MNase-fusions: Taf1, Taf7, Taf13, Spt3 and Spt7. Genes in each table are sorted by signal intensity.

Table S9. *S. cerevisiae* and *S. pombe* strains used in this study.

References

Allen BL, Taatjes DJ. 2015. The Mediator complex: a central integrator of transcription. *Nature Reviews Molecular Cell Biology* **16**:155–166. doi:10.1038/nrm3951

Anders S, Pyl P, Huber W. 2015. HTSeq--a Python framework to work with high-throughput sequencing data. *Bioinformatics* **31**:166–169. doi:10.1093/bioinformatics/btu638

Baptista T, Grünberg S, Minoungou N, Koster MJ, Timmers MH, Hahn S, Devys D, Tora L. 2017. SAGA Is a General Cofactor for RNA Polymerase II Transcription. *Molecular cell* **68**:130-143.e5. doi:10.1016/j.molcel.2017.08.016

Basehoar AD, Zanton SJ, Pugh FB. 2004. Identification and distinct regulation of yeast TATA box-containing genes. *Cell* **116**:699–709.

Bhaumik S, Green M. 2001. SAGA is an essential in vivo target of the yeast acidic activator Gal4p. *Genes & Development* **15**:1935–1945. doi:10.1101/gad.911401

Bieniossek C, Papai G, Schaffitzel C, Garzoni F, Chaillet M, Scheer E, Papadopoulos P, Tora L, Schultz P, Berger I. 2013. The architecture of human general transcription factor TFIID core complex. *Nature* **493**:699–702. doi:10.1038/nature11791

Bonnet J, Wang C-Y, Baptista T, Vincent SD, Hsiao W-C, Stierle M, Kao C-F, Tora L, Devys D. 2014. The SAGA coactivator complex acts on the whole transcribed genome and is required for RNA polymerase II transcription. *Genes & Development* **28**:1999–2012. doi:10.1101/gad.250225.114

Brachmann C, Davies A, Cost G, Caputo E, Li J, Hieter P, Boeke J. 1998. Designer deletion strains derived from Saccharomyces cerevisiae S288C: a useful set of strains and plasmids for PCR-mediated gene disruption and other applications. *Yeast (Chichester, England)* **14**:115–132. doi:10.1002/(sici)1097-0061(19980130)14:2<115::aid-yea204>3.0.co;2-2

Chan LY, Mugler CF, Heinrich S, Vallotton P, Weis K. 2018. Non-invasive measurement of mRNA decay reveals translation initiation as the major determinant of mRNA stability. *eLife* **7**:2433. doi:10.7554/elife.32536

Daniel JA, Torok MS, Sun Z-W, Schieltz D, Allis DC, Yates JR, Grant PA. 2004. Deubiquitination of histone H2B by a yeast acetyltransferase complex regulates transcription. *The Journal of*

biological chemistry **279**:1867–1871. doi:10.1074/jbc.c300494200

Donczew R, Hahn S. 2018. Mechanistic Differences in Transcription Initiation at TATA-Less and TATA-Containing Promoters. *Molecular and Cellular Biology* **38**. doi:10.1128/mcb.00448-17

Doyon Y, Côté J. 2004. The highly conserved and multifunctional NuA4 HAT complex. *Current opinion in genetics & development* **14**:147–154. doi:10.1016/j.gde.2004.02.009

Dudley A, Rougeulle C, Winston F. 1999. The Spt components of SAGA facilitate TBP binding to a promoter at a post-activator-binding step in vivo. *Gene Dev* **13**:2940–2945. doi:10.1101/gad.13.22.2940

Duffy EE, Rutenberg-Schoenberg M, Stark CD, Kitchen RR, Gerstein MB, Simon MD. 2015. Tracking Distinct RNA Populations Using Efficient and Reversible Covalent Chemistry. *Molecular cell* **59**:858–866. doi:10.1016/j.molcel.2015.07.023

Duffy EE, Simon MD. 2016. Enriching s(4) U-RNA Using Methane Thiosulfonate (MTS) Chemistry. *Current protocols in chemical biology* **8**:234–250. doi:10.1002/cpch.12

Grant P, Schieltz D, Pray-Grant M, Steger D, Reese J, Yates J, Workman J. 1998. A subset of TAF(II)s are integral components of the SAGA complex required for nucleosome acetylation and transcriptional stimulation. *Cell* **94**:45–53.

Grünberg S, Henikoff S, Hahn S, Zentner GE. 2016. Mediator binding to UASs is broadly uncoupled from transcription and cooperative with TFIID recruitment to promoters. *The EMBO Journal* **35**:2435–2446. doi:10.15252/embj.201695020

Hahn S, Young ET. 2011. Transcriptional regulation in Saccharomyces cerevisiae: transcription factor regulation and function, mechanisms of initiation, and roles of activators and coactivators. *Genetics* **189**:705–736. doi:10.1534/genetics.111.127019

Haimovich G, Medina DA, Causse SZ, Garber M, Millán-Zambrano G, Barkai O, Chávez S, Pérez-Ortín JE, Darzacq X, Choder M. 2013. Gene expression is circular: factors for mRNA degradation also foster mRNA synthesis. *Cell* **153**:1000–1011. doi:10.1016/j.cell.2013.05.012

Han Y, Luo J, Ranish J, Hahn S. 2014. Architecture of the Saccharomyces cerevisiae SAGA transcription coactivator complex. *The EMBO Journal* **33**:2534–2546. doi:10.15252/embj.201488638

Hantsche M, Cramer P. 2017. Conserved RNA polymerase II initiation complex structure. *Current Opinion in Structural Biology* **47**:17–22. doi:10.1016/j.sbi.2017.03.013

Heinz S, Benner C, Spann N, Bertolino E, Lin YC, Laslo P, Cheng JX, Murre C, Singh H, Glass CK. 2010. Simple combinations of lineage-determining transcription factors prime cis-regulatory elements required for macrophage and B cell identities. *Molecular cell* **38**:576–589. doi:10.1016/j.molcel.2010.05.004

Helmlinger D, Marguerat S, Villén J, Swaney DL, Gygi SP, Bähler J, Winston F. 2011. Tra1 has specific regulatory roles, rather than global functions, within the SAGA co-activator complex. *The EMBO Journal* **30**:2843–2852. doi:10.1038/emboj.2011.181

Henry KW, Wyce A, Lo W-S, Duggan LJ, Emre TN, Kao C-F, Pillus L, Shilatifard A, Osley M, Berger SL. 2003. Transcriptional activation via sequential histone H2B ubiquitylation and deubiquitylation, mediated by SAGA-associated Ubp8. *Genes & Development* **17**:2648–2663. doi:10.1101/gad.1144003

Huisinga KL, Pugh FB. 2004. A genome-wide housekeeping role for TFIID and a highly regulated stress-related role for SAGA in Saccharomyces cerevisiae. *Molecular cell* **13**:573–585.

Joo Y, Ficarro SB, ares L, Chun Y, Marto JA, Buratowski S. 2017. Downstream promoter interactions of TFIID TAFs facilitate transcription reinitiation. *Genes & Development* **31**:2162–2174. doi:10.1101/gad.306324.117

Kamenova I, Warfield L, Hahn S. 2014. Mutations on the DNA binding surface of TBP discriminate between yeast TATA and TATA-less gene transcription. *Molecular and Cellular Biology* **34**:2929–2943. doi:10.1128/mcb.01685-13

Kolesnikova O, Ben-Shem A, Luo J, Ranish J, Schultz P, Papai G. 2018. Molecular structure of promoter-bound yeast TFIID. *Nature communications* **9**:4666. doi:10.1038/s41467-018-07096-y

Koutelou E, Hirsch CL, Dent SY. 2010. Multiple faces of the SAGA complex. *Current opinion in cell biology* **22**:374–382. doi:10.1016/j.ceb.2010.03.005

Kuras L, Kosa P, Mencia M, Struhl K. 2000. TAF-Containing and TAF-independent forms of transcriptionally active TBP in vivo. *Science (New York, NY)* **288**:1244–1248.

Laprade L, Rose D, Winston F. 2007. Characterization of new Spt3 and TATA-binding protein mutants of Saccharomyces cerevisiae: Spt3 TBP allele-specific interactions and bypass of Spt8. *Genetics* **177**:2007–2017. doi:10.1534/genetics.107.081976

Larschan E, Winston F. 2001. The S. cerevisiae SAGA complex functions in vivo as a coactivator for transcriptional activation by Gal4. *Gene Dev* **15**:1946–1956. doi:10.1101/gad.911501

Lee KK, Sardiu ME, Swanson SK, Gilmore JM, Torok M, Grant PA, Florens L, Workman JL, Washburn MP. 2011. Combinatorial depletion analysis to assemble the network architecture of the SAGA and ADA chromatin remodeling complexes. *Molecular Systems Biology* **7**:503. doi:10.1038/msb.2011.40

Lee T, Causton H, Holstege F, Shen W, Hannett N, Jennings E, Winston F, Green M, Young R. 2000. Redundant roles for the TFIID and SAGA complexes in global transcription. *Nature* **405**:701–704. doi:10.1038/35015104

Li X, Bhaumik S, Green M. 2000. Distinct classes of yeast promoters revealed by differential TAF recruitment. *Science (New York, NY)* **288**:1242–1244.

Liu G, Zheng X, Guan H, Cao Y, Qu H, Kang J, Ren X, Lei J, Dong M-Q, Li X, Li H. 2019. Architecture of Saccharomyces cerevisiae SAGA complex. *Cell discovery* **5**:25. doi:10.1038/s41421-019-0094-x

Louder RK, He Y, López-Blanco J, Fang J, Chacón P, Nogales E. 2016. Structure of promoter-bound TFIID and model of human pre-initiation complex assembly. *Nature* **531**:604–609. doi:10.1038/nature17394

Mohibullah N, Hahn S. 2008. Site-specific cross-linking of TBP in vivo and in vitro reveals a direct functional interaction with the SAGA subunit Spt3. *Genes & Development* **22**:2994–3006. doi:10.1101/gad.1724408

Moqtaderi Z, Bai Y, Poon D, Weil P, Struhl K. 1996. TBP-associated factors are not generally required for transcriptional activation in yeast. *Nature* **383**:188–191. doi:10.1038/383188a0

Morris SA, Rao B, Garcia BA, Hake SB, Diaz RL, Shabanowitz J, Hunt DF, Allis DC, Lieb JD, Strahl BD. 2007. Identification of histone H3 lysine 36 acetylation as a highly conserved histone modification. *The Journal of biological chemistry* **282**:7632–7640. doi:10.1074/jbc.m607909200

Munchel SE, Shultzaberger RK, Takizawa N, Weis K. 2011. Dynamic profiling of mRNA turnover reveals gene-specific and system-wide regulation of mRNA decay. *Molecular Biology of the Cell* **22**:2787–2795. doi:10.1091/mbc.e11-01-0028

Nishimura K, Fukagawa T, Takisawa H, Kakimoto T, Kanemaki M. 2009. An auxin-based degron system for the rapid depletion of proteins in nonplant cells. *Nature Methods* **6**:917–922. doi:10.1038/nmeth.1401

Nogales E, Louder RK, He Y. 2017. Structural Insights into the Eukaryotic Transcription Initiation Machinery. *Annual review of biophysics* **46**:59–83. doi:10.1146/annurev-biophys-070816-033751

O'Duibhir E, Lijnzaad P, Benschop JJ, Lenstra TL, van Leenen D, Koerkamp MJ, Margaritis T, Brok MO, Kemmeren P, Holstege FC. 2014. Cell cycle population effects in perturbation studies. *Molecular Systems Biology* **10**:732. doi:10.15252/msb.20145172

Papai G, Frechard A, Kolesnikova O, Crucifix C, Schultz P, Ben-Shem A. 2019. Structure of SAGA and mechanism of TBP deposition on gene promoters.

Park D, Morris AR, Battenhouse A, Iyer VR. 2014. Simultaneous mapping of transcript ends at single-nucleotide resolution and identification of widespread promoter-associated non-coding RNA governed by TATA elements. *Nucleic Acids Research* **42**:3736–3749. doi:10.1093/nar/gkt1366

Patel AB, Louder RK, Greber BJ, Grünberg S, Luo J, Fang J, Liu Y, Ranish J, Hahn S, Nogales E. 2018. Structure of human TFIID and mechanism of TBP loading onto promoter DNA. *Science (New York, NY)* **362**:eaau8872. doi:10.1126/science.aau8872

Petrenko N, Jin Y, Dong L, Wong K, Struhl K. 2019. Requirements for RNA polymerase II preinitiation complex formation in vivo. *eLife* **8**:699. doi:10.7554/elife.43654

Rando OJ, Winston F. 2012. Chromatin and transcription in yeast. *Genetics* **190**:351–387. doi:10.1534/genetics.111.132266

Rhee H, Pugh FB. 2012. Genome-wide structure and organization of eukaryotic pre-initiation complexes. *Nature* **483**:295–301. doi:10.1038/nature10799

Rodriguez J, McKnight JN, Tsukiyama T. 2014. Genome-Wide Analysis of Nucleosome Positions,

Occupancy, and Accessibility in Yeast: Nucleosome Mapping, High-Resolution Histone ChIP, and NCAM. *Curr Protoc Mol Biology* **108**:21.28.1-21.28.16. doi:10.1002/0471142727.mb2128s108

Rodriguez-Navarro S. 2009. Insights into SAGA function during gene expression. *EMBO reports* **10**:843–850. doi:10.1038/embor.2009.168

Sainsbury S, Bernecky C, Cramer P. 2015. Structural basis of transcription initiation by RNA polymerase II. *Nature Reviews Molecular Cell Biology* **16**:129–143. doi:10.1038/nrm3952

Sermwittayawong D, Tan S. 2006. SAGA binds TBP via its Spt8 subunit in competition with DNA: implications for TBP recruitment. *The EMBO Journal* **25**:3791–3800. doi:10.1038/sj.emboj.7601265

Setiaputra D, Ross JD, Lu S, Cheng DT, Dong M-Q, Yip CK. 2015. Conformational flexibility and subunit arrangement of the modular yeast Spt-Ada-Gcn5 acetyltransferase complex. *Journal of Biological Chemistry* **290**:10057–10070. doi:10.1074/jbc.m114.624684

Sprouse RO, Shcherbakova I, Cheng H, Jamison E, Brenowitz M, Auble DT. 2008. Function and structural organization of Mot1 bound to a natural target promoter. *The Journal of biological chemistry* **283**:24935–24948. doi:10.1074/jbc.m803749200

Sterner D, Grant P, Roberts S, Duggan L, Belotserkovskaya R, Pacella L, Winston F, Workman J, Berger S. 1999. Functional organization of the yeast SAGA complex: distinct components involved in structural integrity, nucleosome acetylation, and TATA-binding protein interaction. *Molecular and Cellular Biology* **19**:86–98.

Stewart-Ornstein J, Nelson C, DeRisi J, Weissman JS, El-Samad H. 2013. Msn2 coordinates a stoichiometric gene expression program. *Curr Biology Cb* **23**:2336–45. doi:10.1016/j.cub.2013.09.043

Sun M, Schwalb B, Schulz D, Pirkl N, Etzold S, Larivière L, Maier KC, Seizl M, Tresch A, Cramer P. 2012. Comparative dynamic transcriptome analysis (cDTA) reveals mutual feedback between mRNA synthesis and degradation. *Genome Research* **22**:1350–1359. doi:10.1101/gr.130161.111

Vinayachandran V, Reja R, Rossi MJ, Park B, Rieber L, Mittal C, Mahony S, Pugh FB. 2018. Widespread and precise reprogramming of yeast protein-genome interactions in response to heat shock. *Genome Research*. doi:10.1101/gr.226761.117

Walker S, Reese J, Apone L, Green M. 1996. Transcription activation in cells lacking TAFIIS. *Nature* **383**:185–188. doi:10.1038/383185a0

Warfield L, Ramachandran S., Baptista T, Devys D, Tora L, Hahn S. 2017. Transcription of Nearly All Yeast RNA Polymerase II-Transcribed Genes Is Dependent on Transcription Factor TFIID. *Molecular cell* **68**:118-129.e5. doi:10.1016/j.molcel.2017.08.014

Zentner GE, Kasinathan S, Xin B, Rohs R, Henikoff S. 2015. ChEC-seq kinetics discriminates transcription factor binding sites by DNA sequence and shape in vivo. *Nature communications* **6**:8733. doi:10.1038/ncomms9733

A

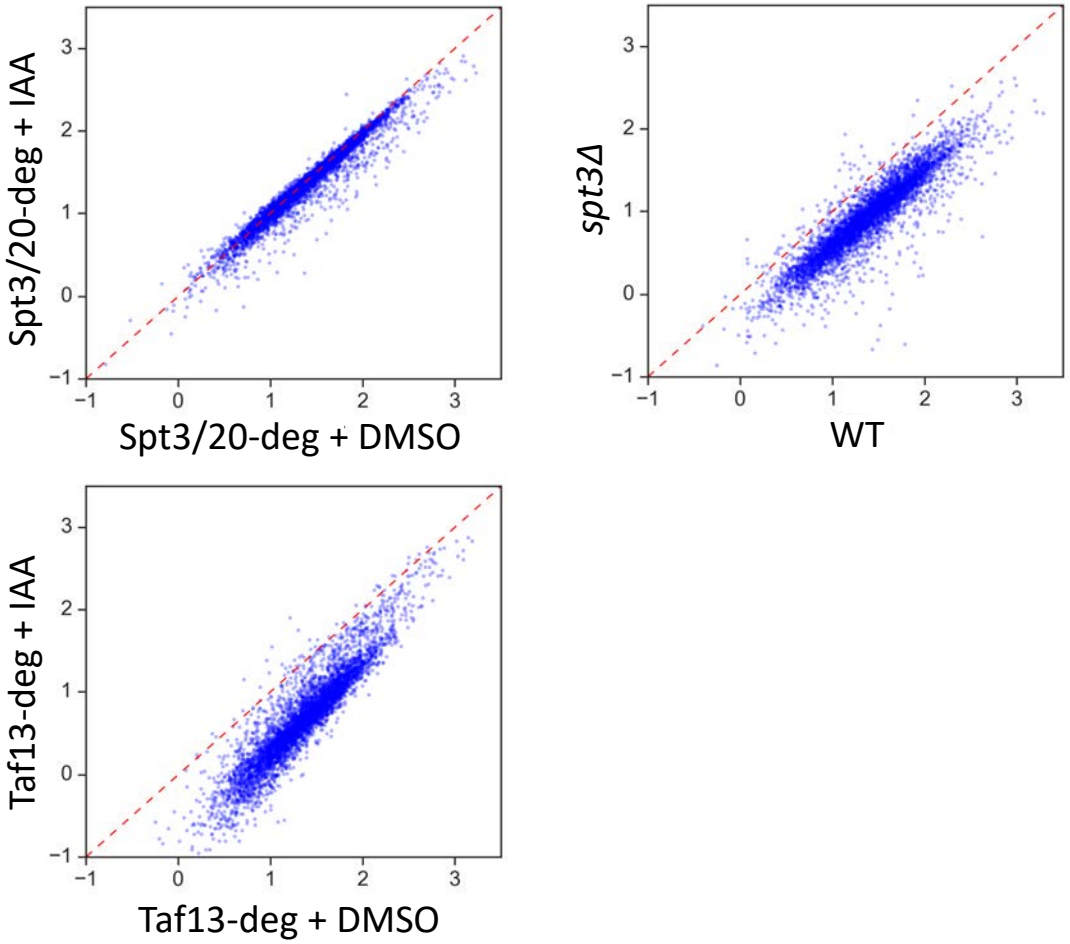
Spt3/20-deg + IAA
Spt3/20-deg + DMSO
spt3Δ
WT
Taf13-deg + IAA
Taf13-deg + DMSO

B

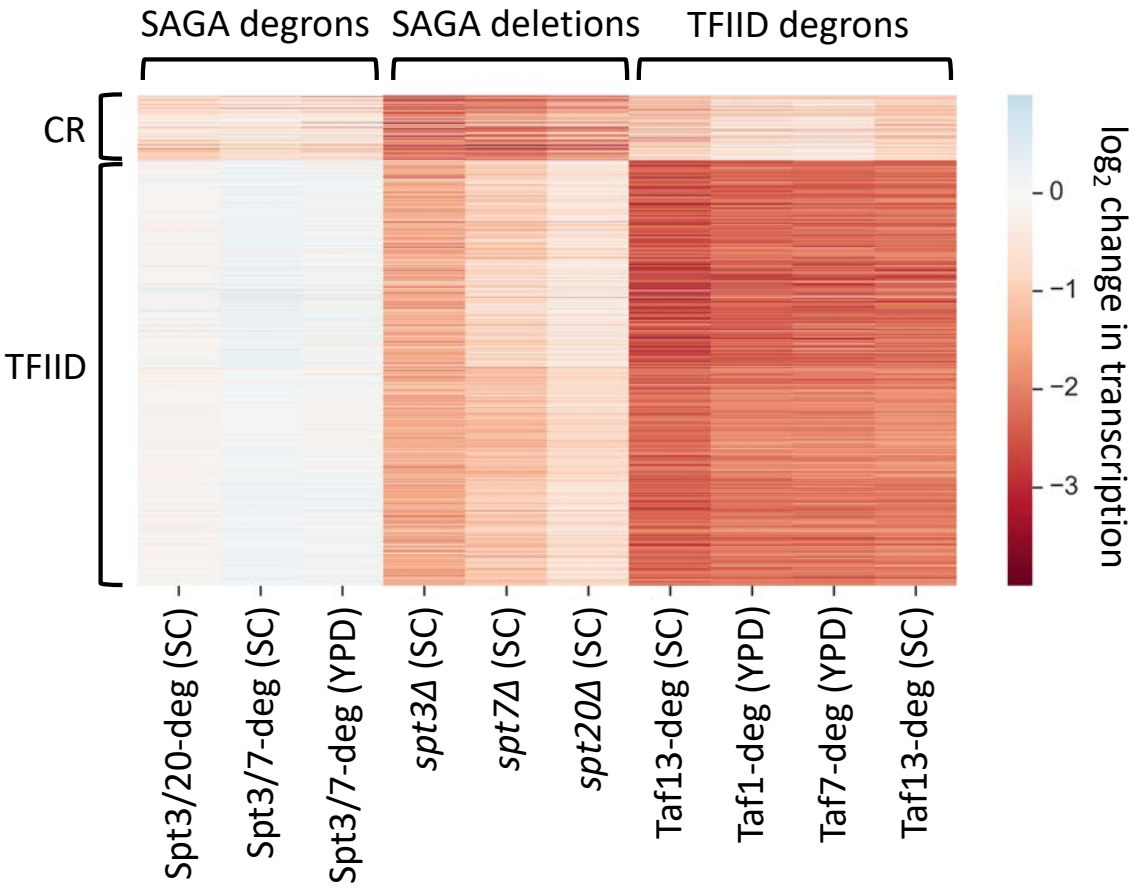
SAGA degrons
SAGA deletions
TFIID degrons
CR
TFIID
log2 change in transcription
Spt3/20-deg (SC)
Spt3/7-deg (SC)
Spt3/7-deg (YPD)
spt3Δ (SC)
spt7Δ (SC)
spt20Δ (SC)
Taf13-deg (SC)
Taf1-deg (YPD)
Taf7-deg (YPD)
Taf13-deg (SC)

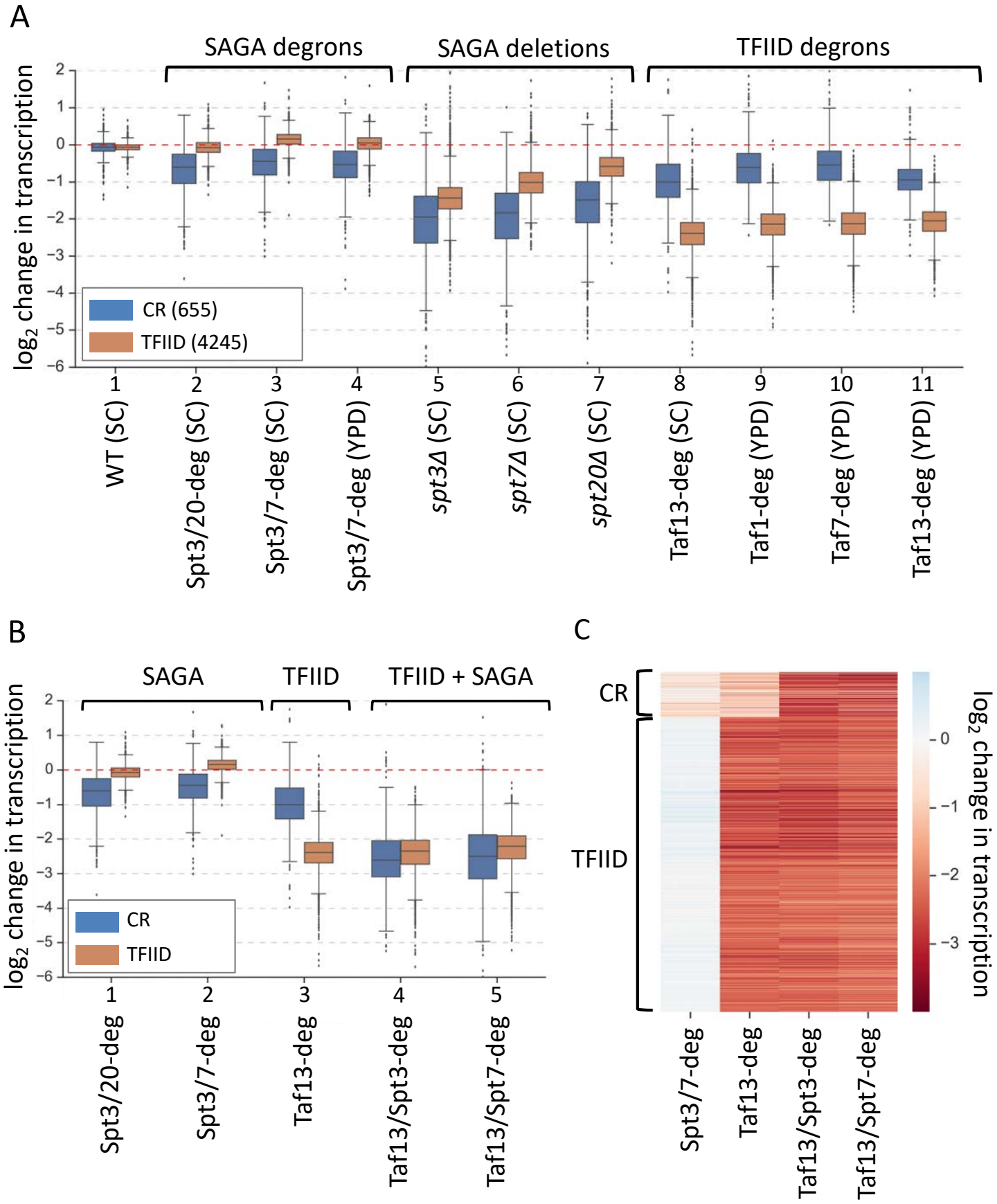
A
SAGA degrons
SAGA deletions
TFIID degrons
log2 change in transcription
CR (655)
TFIID (4245)
1 WT (SC)
2 Spt3/20-deg (SC)
3 Spt3/7-deg (SC)
4 Spt3/7-deg (YPD)
5 spt3Δ (SC)
6 spt7Δ (SC)
7 spt20Δ (SC)
8 Taf13-deg (SC)
9 Taf1-deg (YPD)
10 Taf7-deg (YPD)
11 Taf13-deg (YPD)
B
SAGA
TFIID
TFIID + SAGA
log2 change in transcription
CR
TFIID
1 Spt3/20-deg
2 Spt3/7-deg
3 Taf13-deg
4 Taf13/Spt3-deg
5 Taf13/Spt7-deg
C
CR
TFIID
log2 change in transcription
Spt3/7-deg
Taf13-deg
Taf13/Spt3-deg
Taf13/Spt7-deg

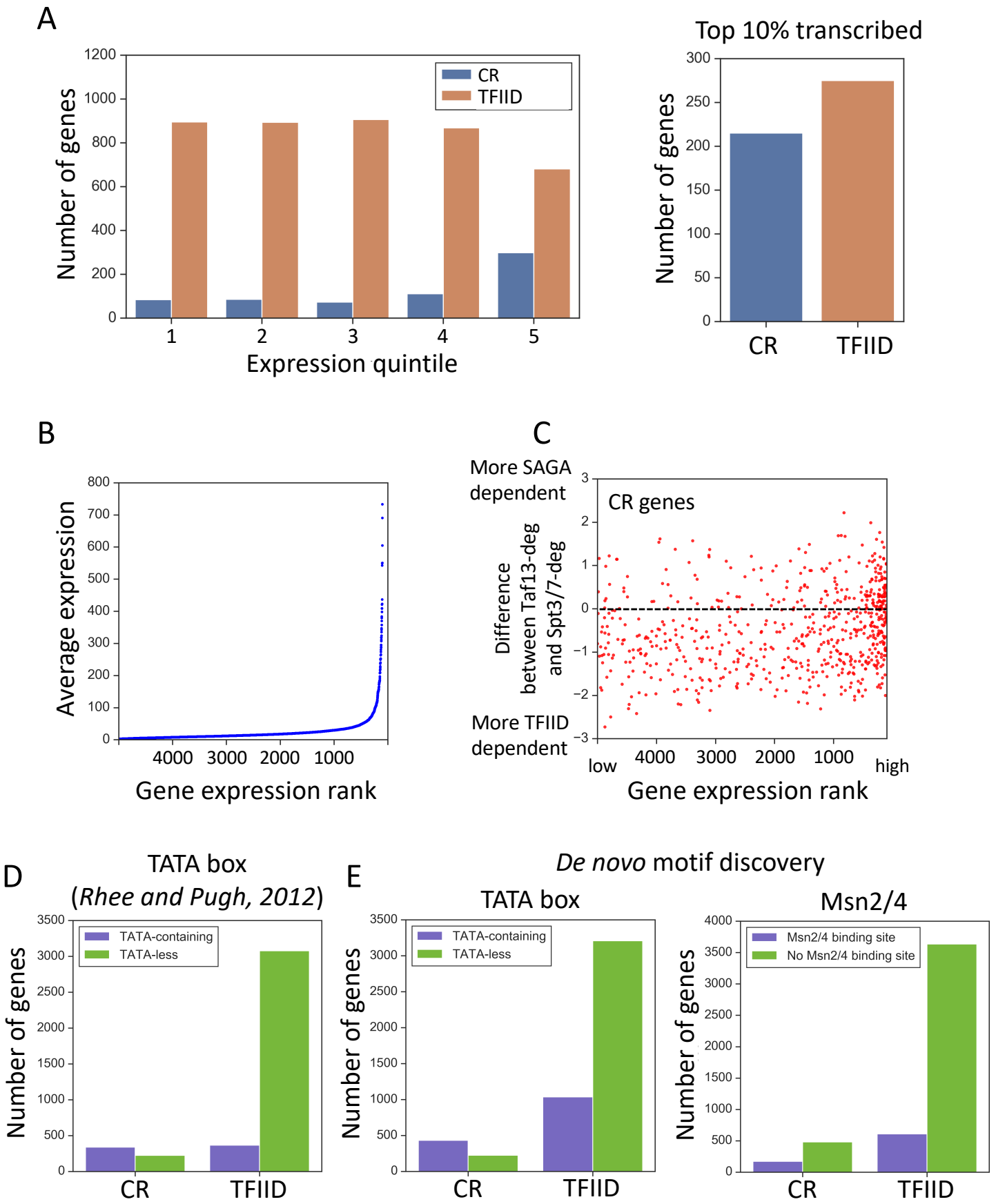
A
Number of genes
Expression quintile
CR
TFIID
Top 10% transcribed
B
Average expression
Gene expression rank
C
More SAGA dependent
More TFIID dependent
CR genes
Difference between Taf13-deg and Spt3/7-deg
low
high
Gene expression rank
D
TATA box
(Rhee and Pugh, 2012)
TATA-containing
TATA-less
E
De novo motif discovery
TATA box
Msn2/4
Msn2/4 binding site
No Msn2/4 binding site

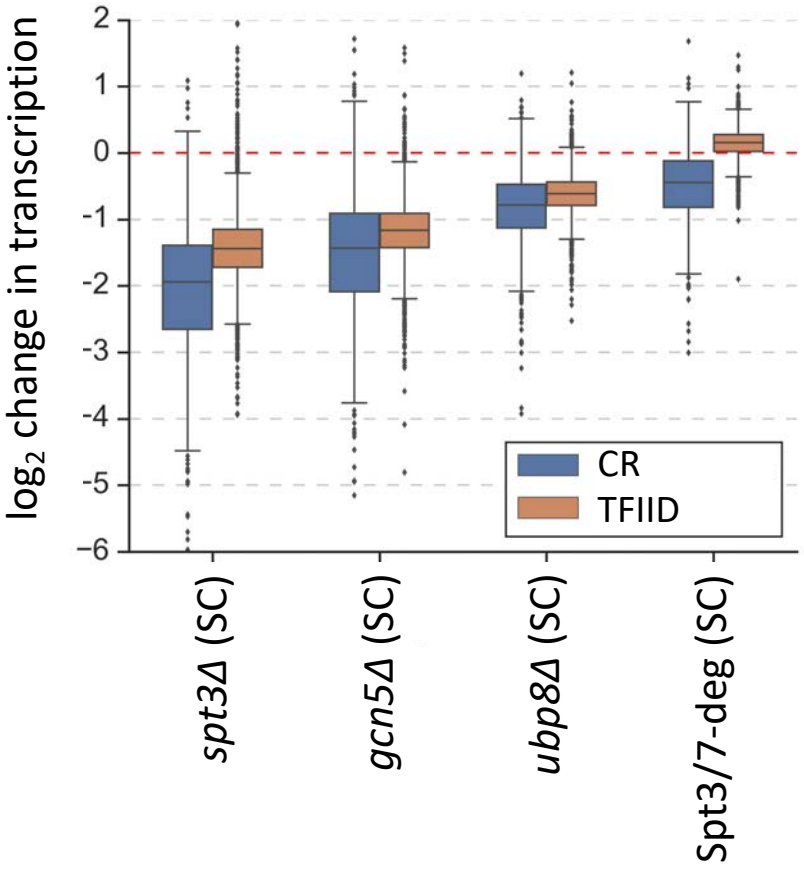
log2 change in transcription
2
1
0
-1
-2
-3
-4
-5
−6
CR
TFIID
spt3Δ (SC)
gcn5Δ (SC)
ubp8Δ (SC)
Spt3/7-deg (SC)

A SAGA deletions

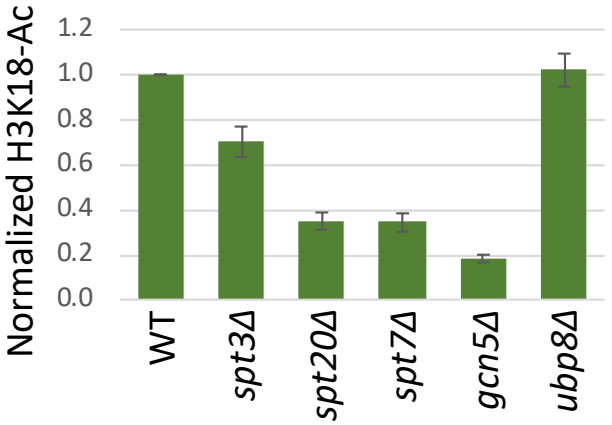

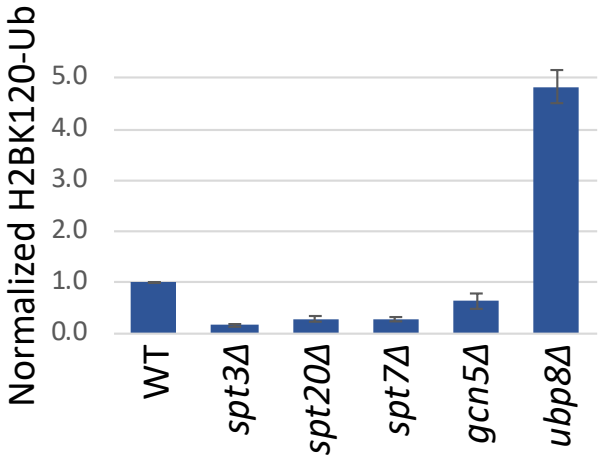

B SAGA degrons

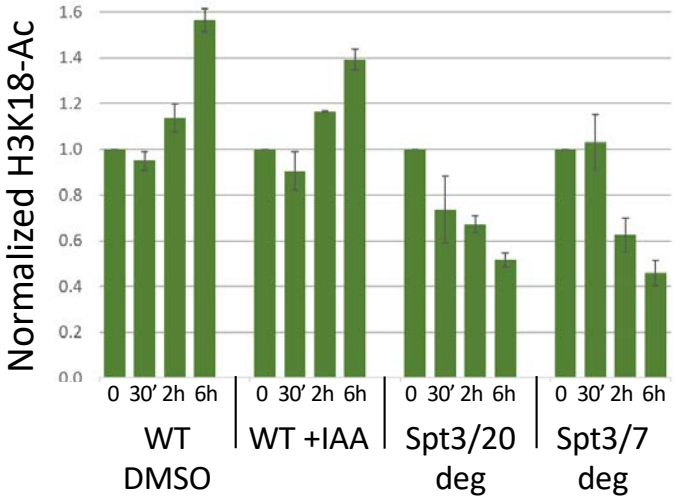

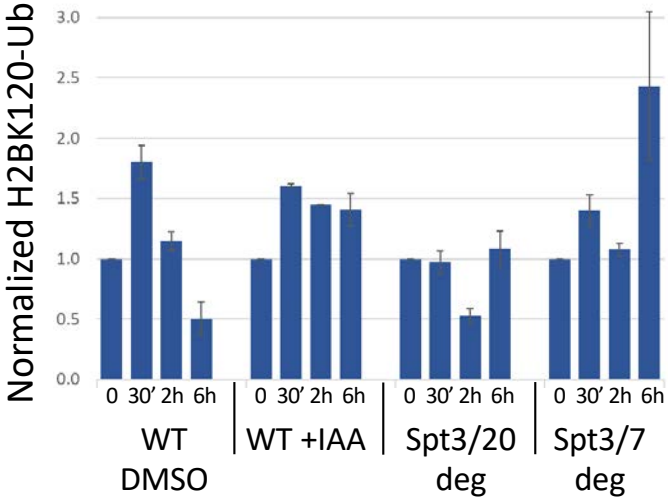

C

H3K18-Ac ChIP-seq

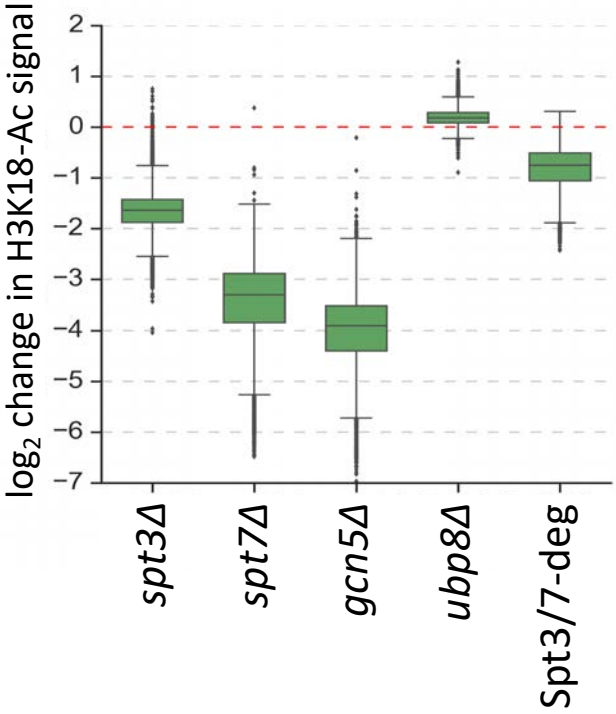

A

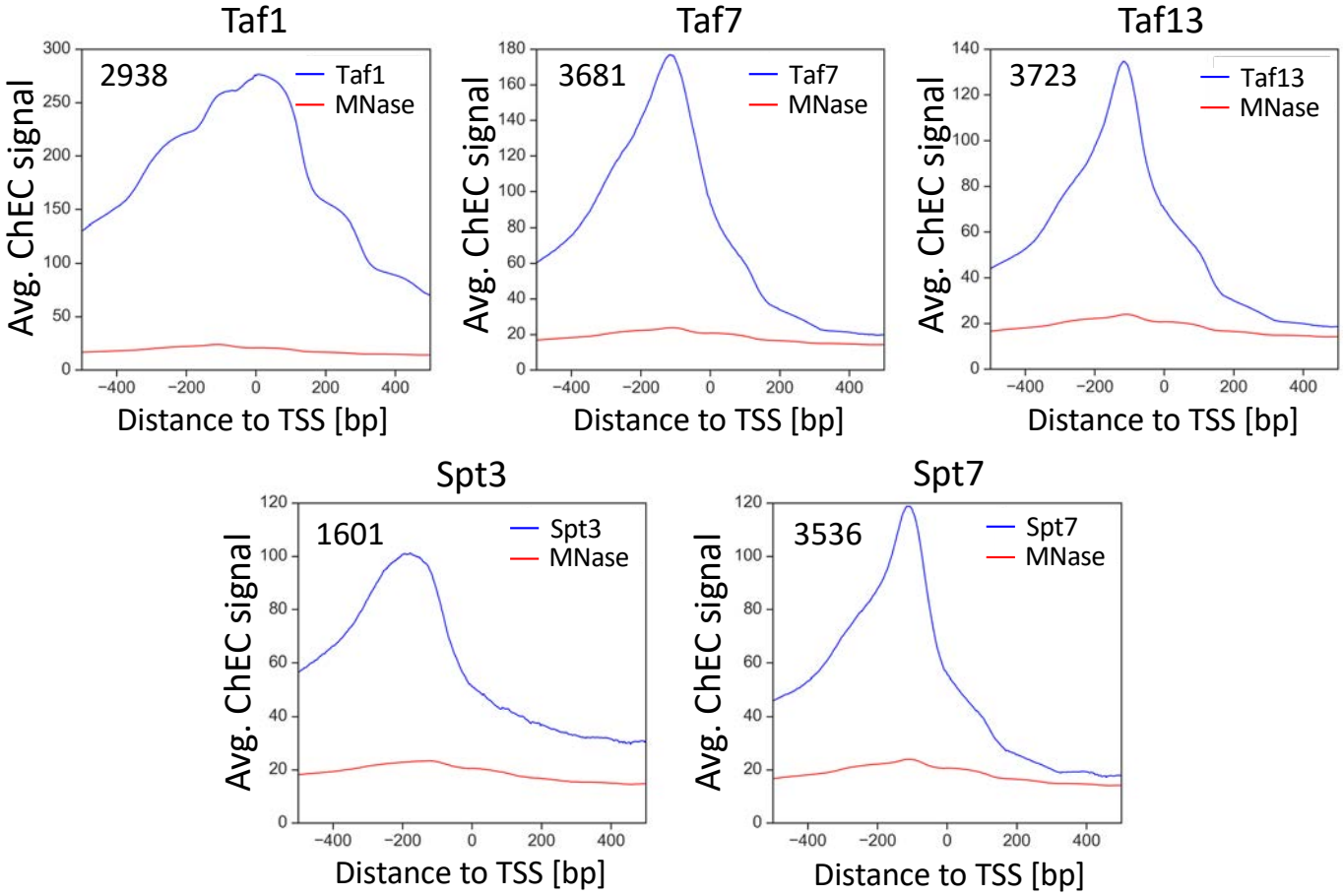
Taf1
2938
Taf1
MNase
Avg. ChEC signal
Distance to TSS [bp]
Taf7
3681
Taf7
MNase
Avg. ChEC signal
Distance to TSS [bp]
Taf13
3723
Taf13
MNase
Avg. ChEC signal
Distance to TSS [bp]
Spt3
1601
Spt3
MNase
Avg. ChEC signal
Distance to TSS [bp]
Spt7
3536
Spt7
MNase
Avg. ChEC signal
Distance to TSS [bp]

B

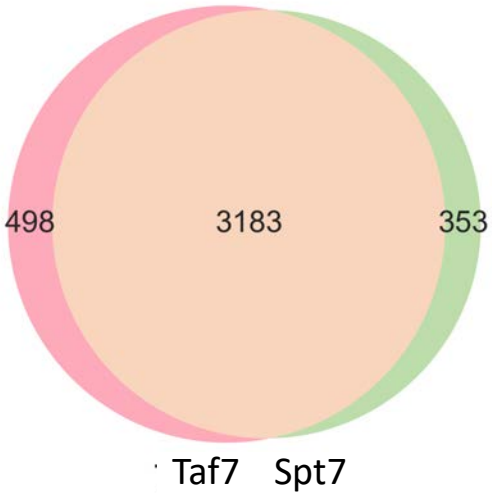
498
3183
353
Taf7
Spt7

C

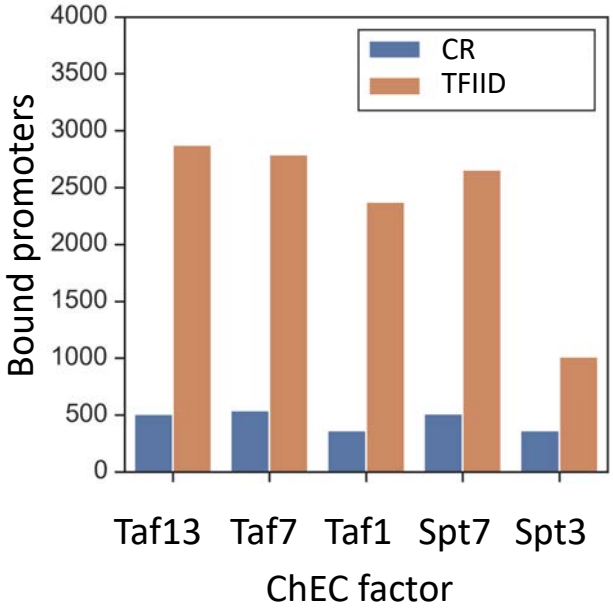
CR
TFIID
Bound promoters
Taf13
Taf7
Taf1
Spt7
Spt3
ChEC factor

A

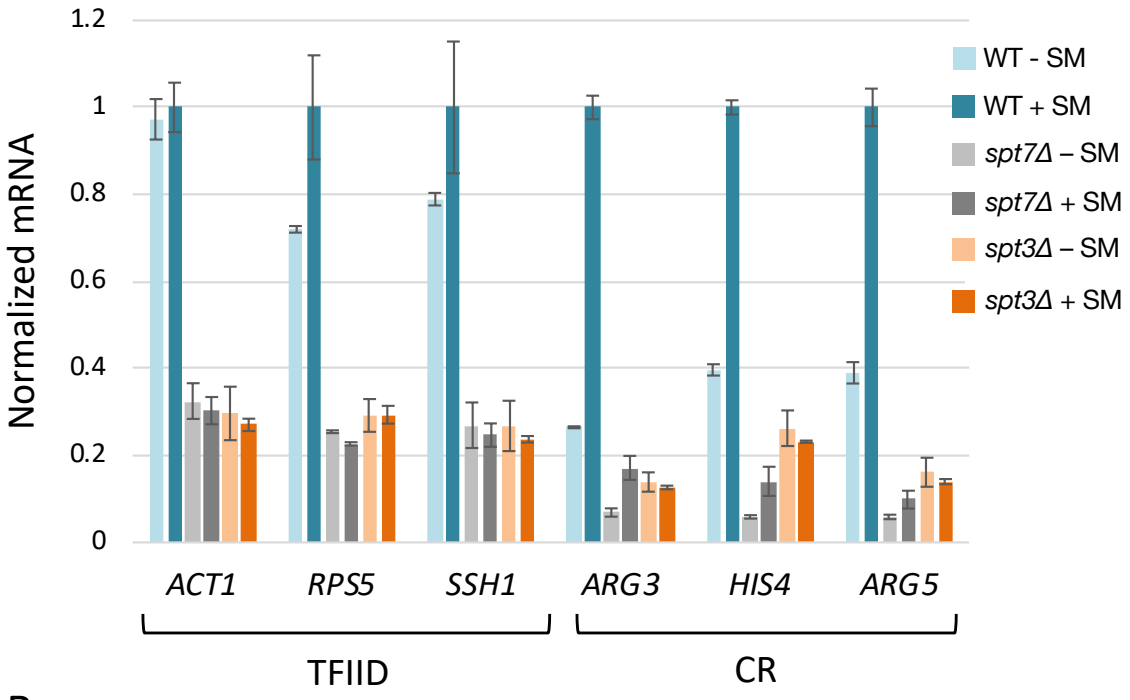
1.2
1
0.8
0.6
0.4
0.2
0
Normalized mRNA
WT - SM
WT + SM
spt7Δ – SM
spt7Δ + SM
spt3Δ – SM
spt3Δ + SM
ACT1
RPS5
SSH1
ARG3
HIS4
ARG5
TFIID
CR

B

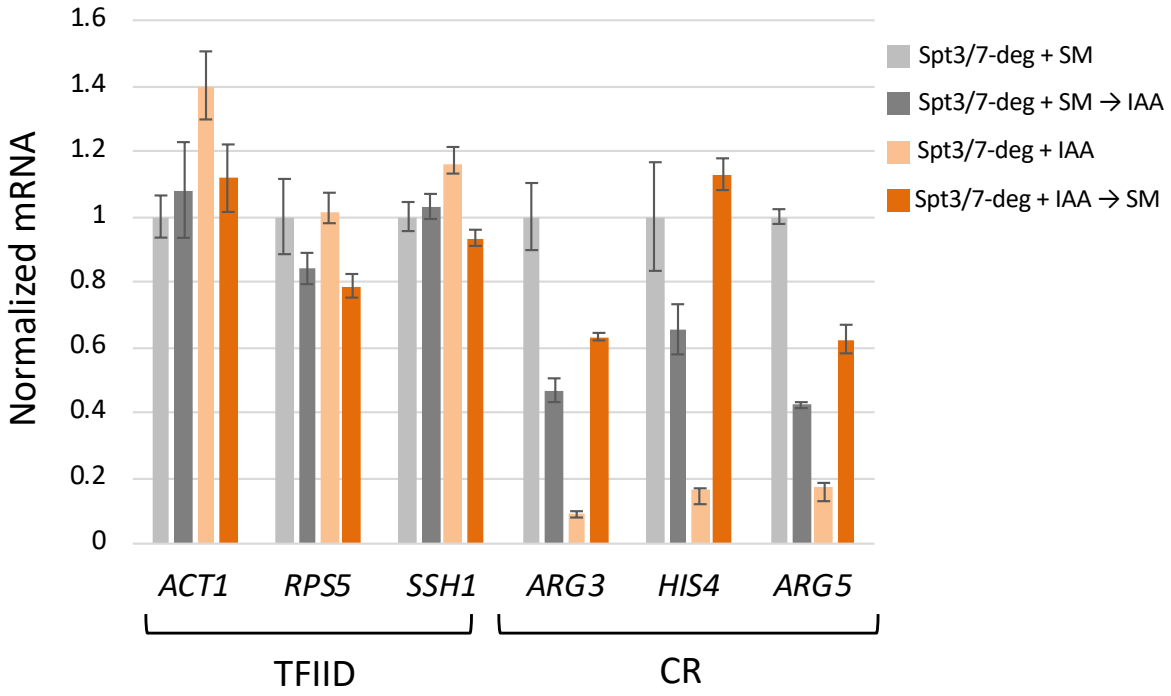
1.6
1.4
1.2
1
0.8
0.6
0.4
0.2
0
Normalized mRNA
Spt3/7-deg + SM
Spt3/7-deg + SM → IAA
Spt3/7-deg + IAA
Spt3/7-deg + IAA → SM
ACT1
RPS5
SSH1
ARG3
HIS4
ARG5
TFIID
CR

Figure 8

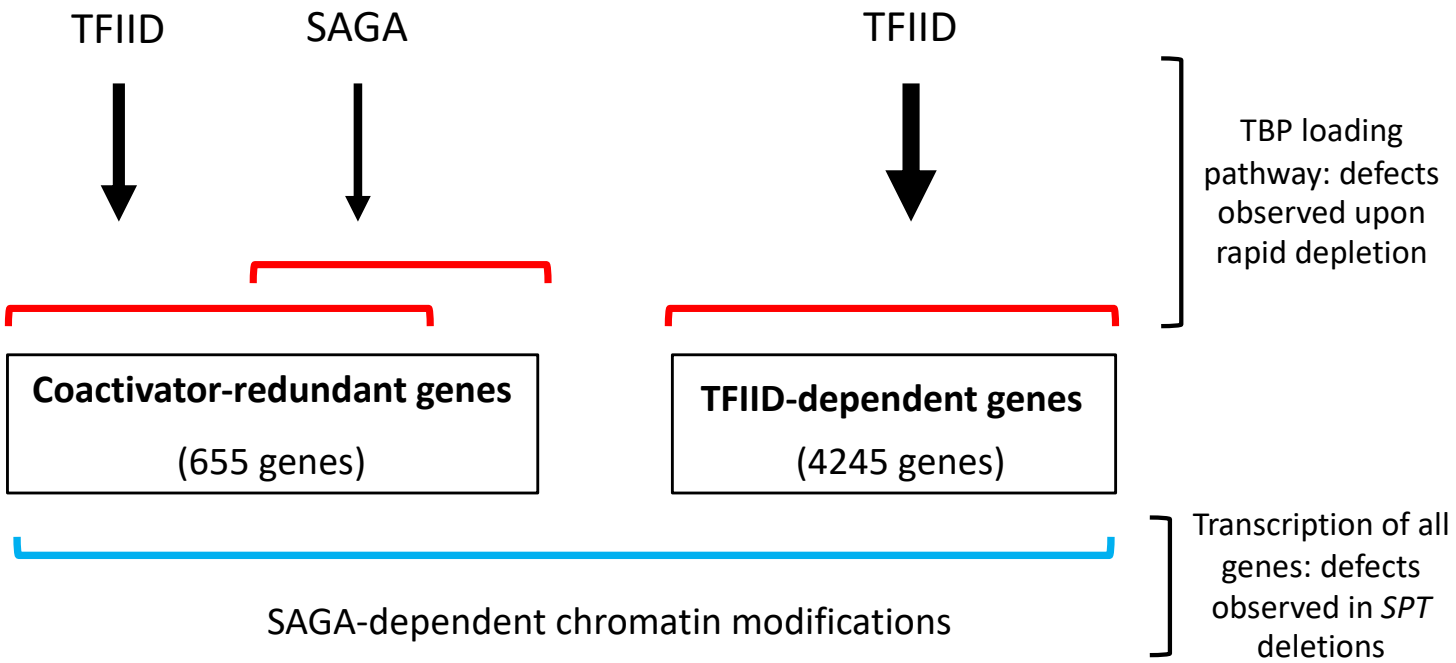
TFIID
SAGA
TFIID
TBP loading pathway: defects observed upon rapid depletion
Coactivator-redundant genes
(655 genes)
TFIID-dependent genes
(4245 genes)
Transcription of all genes: defects observed in *SPT* deletions
SAGA-dependent chromatin modifications

A

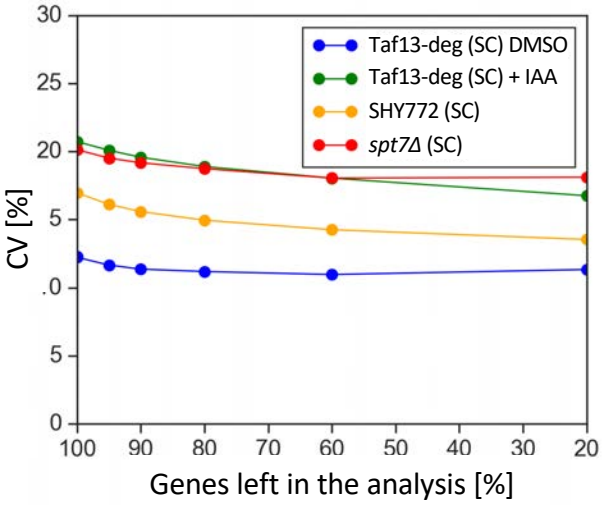
Taf13-deg (SC) DMSO
Taf13-deg (SC) + IAA
SHY772 (SC)
spt7Δ (SC)
CV [%]
Genes left in the analysis [%]

B

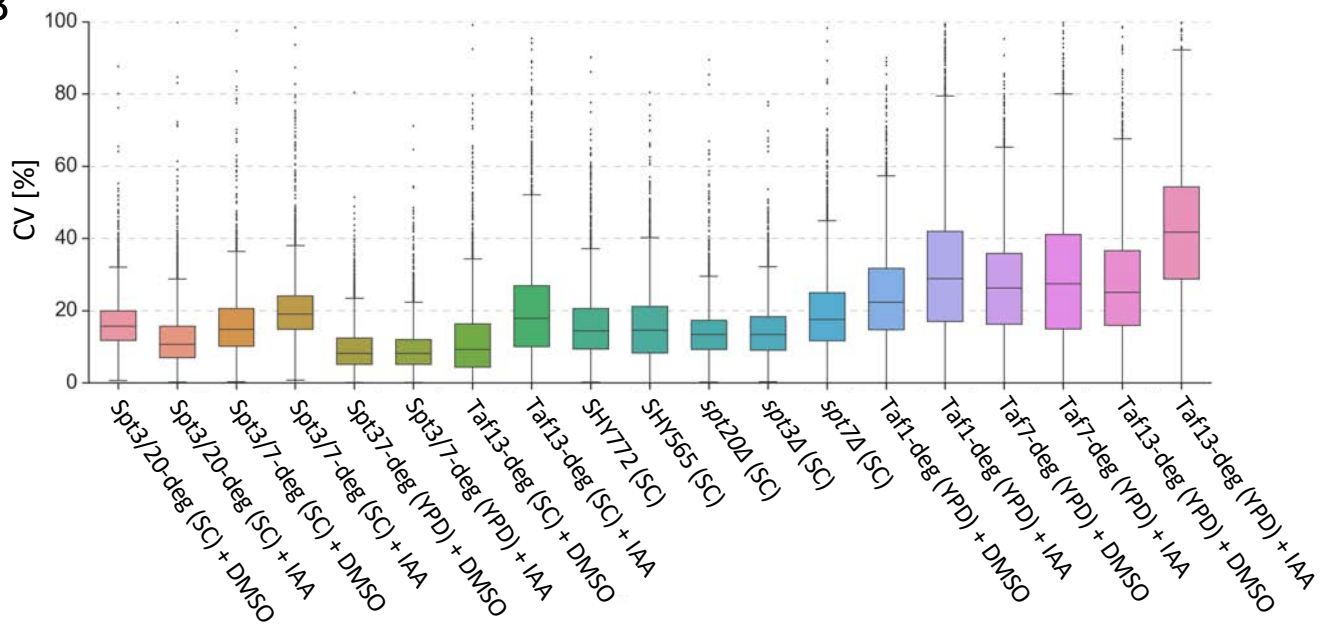
CV [%]
Spt3/20-deg (SC) + DMSO
Spt3/20-deg (SC) + IAA
Spt3/7-deg (SC) + DMSO
Spt3/7-deg (SC) + IAA
Spt37-deg (YPD) + DMSO
Spt3/7-deg (YPD) + IAA
Taf13-deg (SC) + DMSO
Taf13-deg (SC) + IAA
SHY772 (SC)
SHY565 (SC)
spt20Δ (SC)
spt3Δ (SC)
spt7Δ (SC)
Taf1-deg (YPD) + DMSO
Taf1-deg (YPD) + IAA
Taf7-deg (YPD) + DMSO
Taf7-deg (YPD) + IAA
Taf13-deg (YPD) + DMSO
Taf13-deg (YPD) + IAA

A

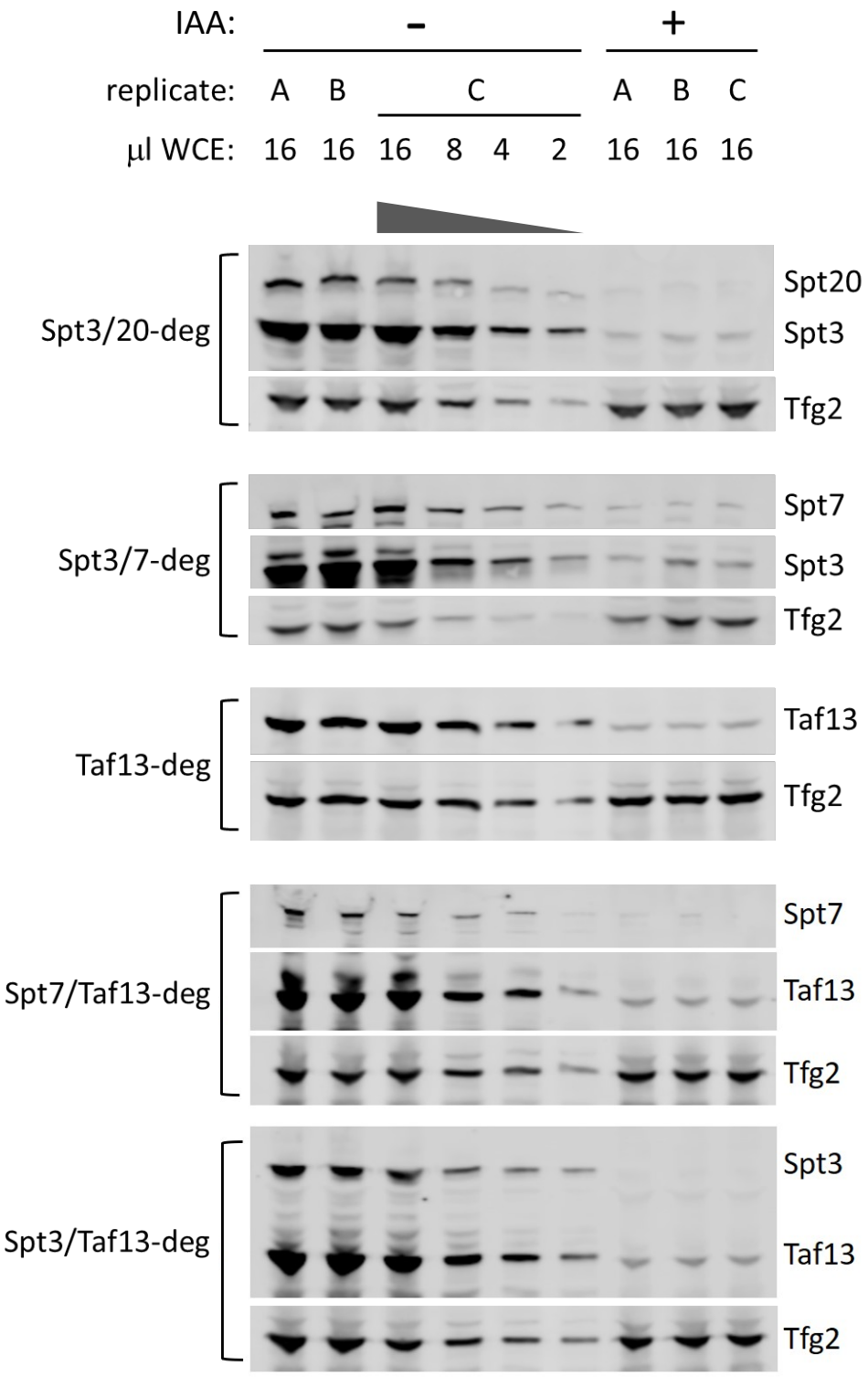
IAA: - +
replicate: A B C A B C
µl WCE: 16 16 16 8 4 2 16 16 16
Spt3/20-deg
Spt20
Spt3
Tfg2
Spt3/7-deg
Spt7
Spt3
Tfg2
Taf13-deg
Taf13
Tfg2
Spt7/Taf13-deg
Spt7
Taf13
Tfg2
Spt3/Taf13-deg
Spt3
Taf13
Tfg2

B

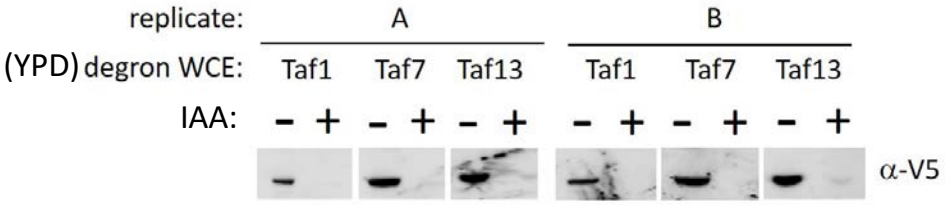
replicate: A B
(YPD) degron WCE: Taf1 Taf7 Taf13 Taf1 Taf7 Taf13
IAA: - + - + - + - + - + - +
α-V5

A

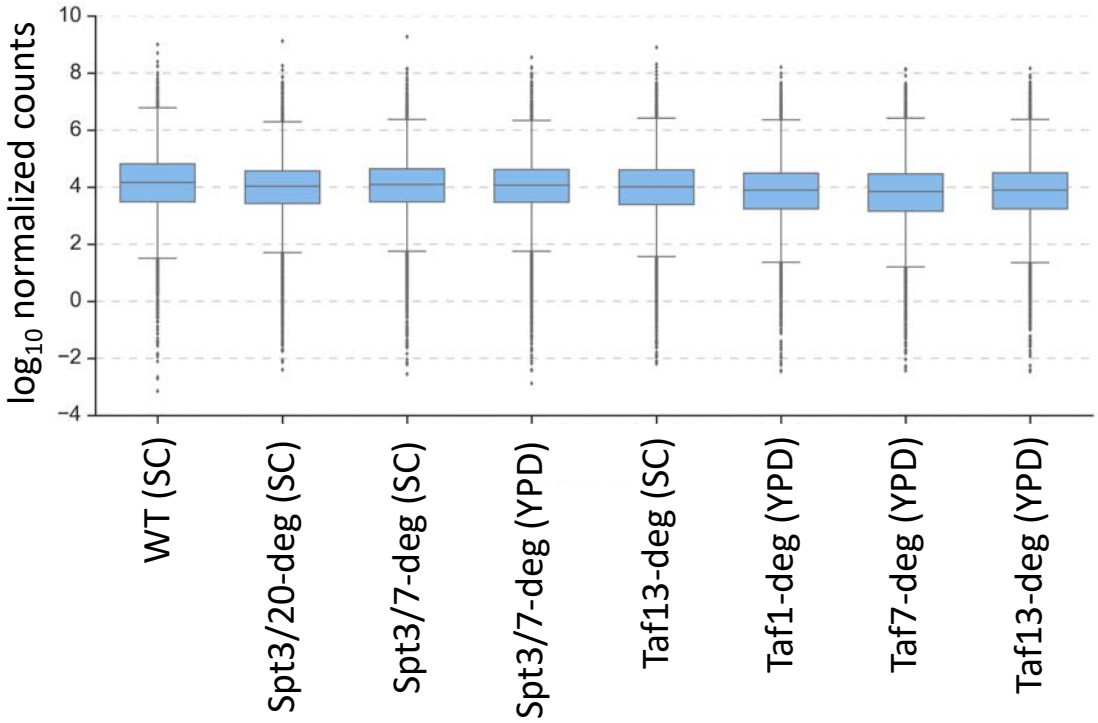
log10 normalized counts
10
8
6
4
2
0
−2
−4
WT (SC)
Spt3/20-deg (SC)
Spt3/7-deg (SC)
Spt3/7-deg (YPD)
Taf13-deg (SC)
Taf1-deg (YPD)
Taf7-deg (YPD)
Taf13-deg (YPD)

B

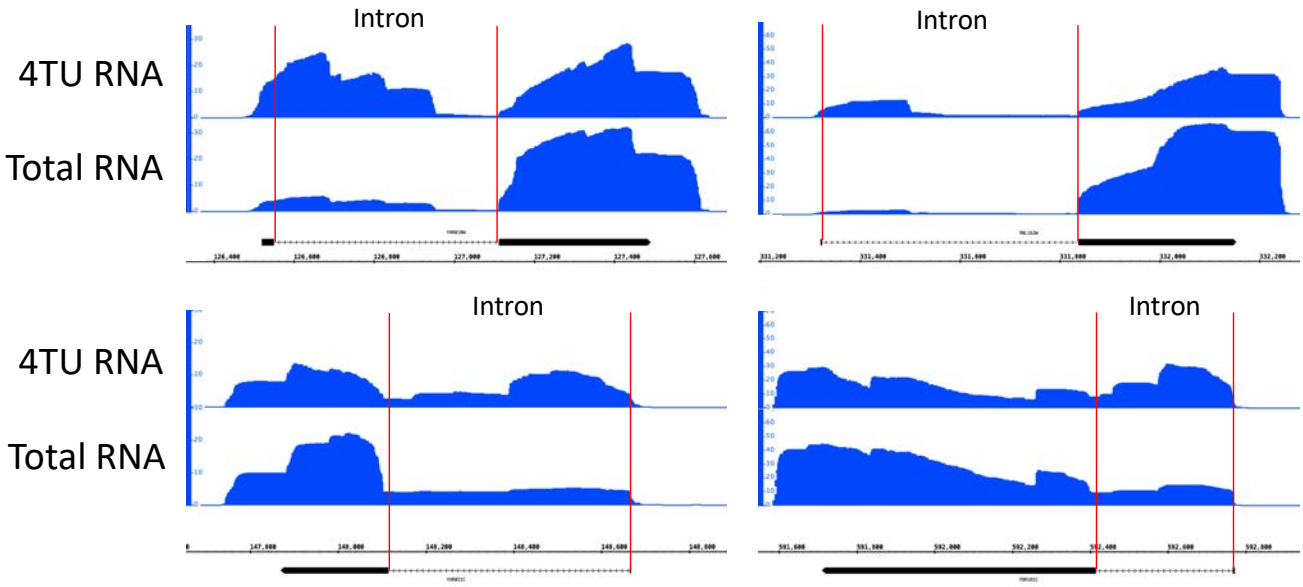
4TU RNA
Total RNA
Intron
Intron
4TU RNA
Total RNA
Intron
Intron

A

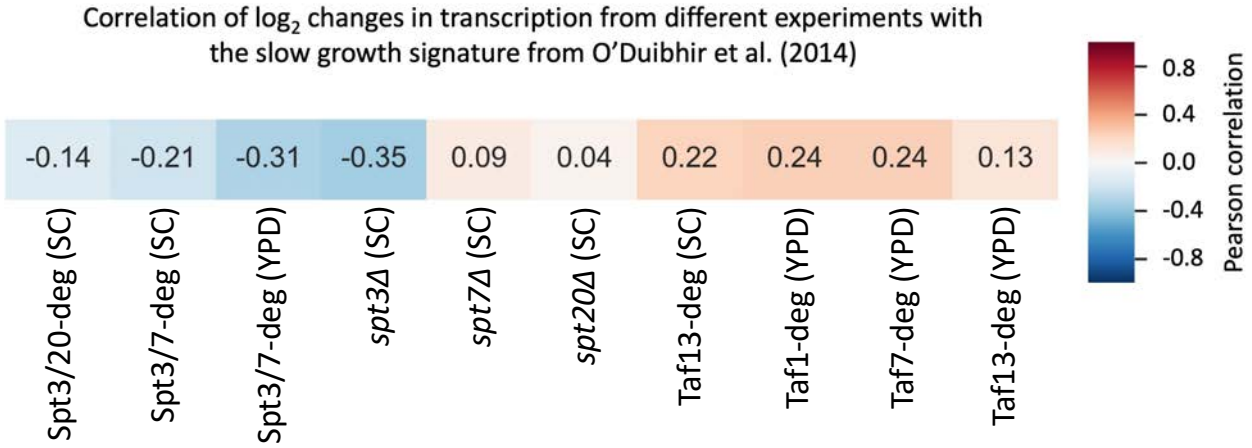
Correlation of log2 changes in transcription from different experiments with the slow growth signature from O'Duibhir et al. (2014)
-0.14
-0.21
-0.31
-0.35
0.09
0.04
0.22
0.24
0.24
0.13
Spt3/20-deg (SC)
Spt3/7-deg (SC)
Spt3/7-deg (YPD)
spt3Δ (SC)
spt7Δ (SC)
spt20Δ (SC)
Taf13-deg (SC)
Taf1-deg (YPD)
Taf7-deg (YPD)
Taf13-deg (YPD)
0.8
0.4
0.0
-0.4
-0.8
Pearson correlation

B

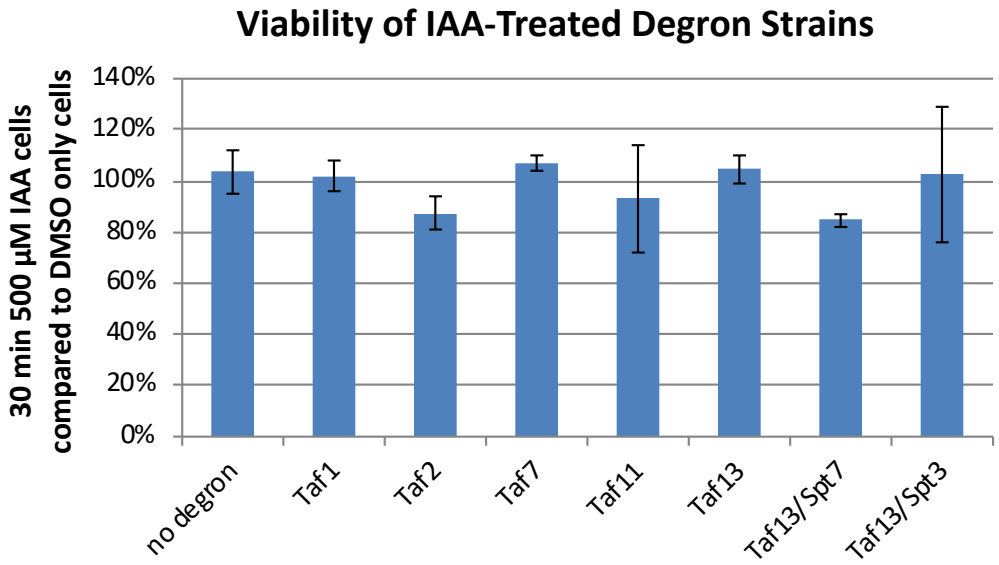
Viability of IAA-Treated Degron Strains
30 min 500 µM IAA cells compared to DMSO only cells
140%
120%
100%
80%
60%
40%
20%
0%
no degron
Taf1
Taf2
Taf7
Taf11
Taf13
Taf13/Spt7
Taf13/Spt3

C

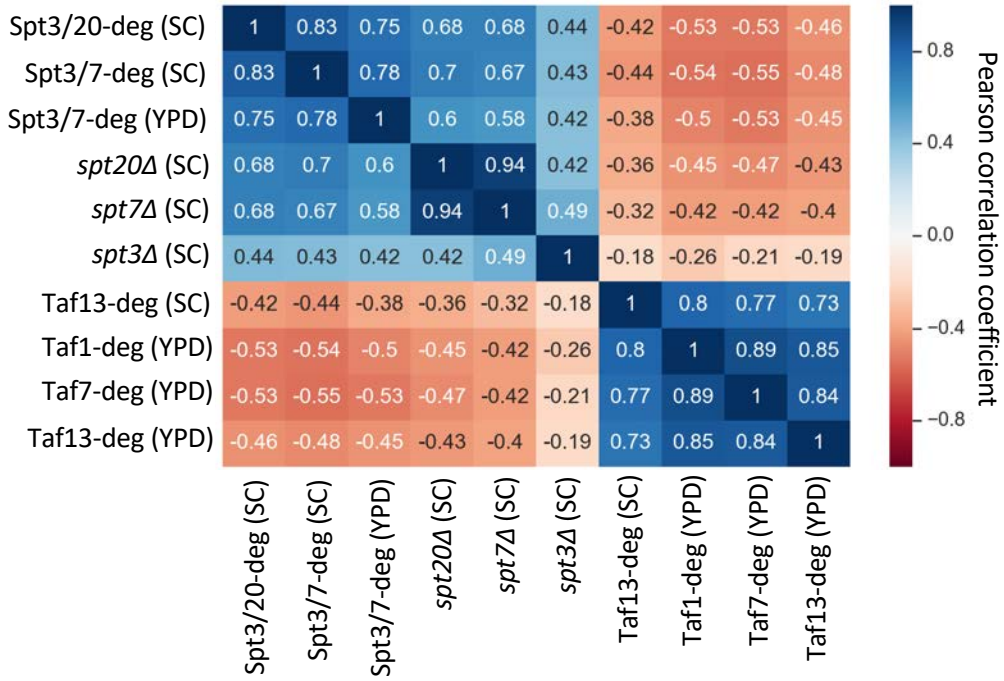
Spt3/20-deg (SC) 1 0.83 0.75 0.68 0.68 0.44 -0.42 -0.53 -0.53 -0.46
Spt3/7-deg (SC) 0.83 1 0.78 0.7 0.67 0.43 -0.44 -0.54 -0.55 -0.48
Spt3/7-deg (YPD) 0.75 0.78 1 0.6 0.58 0.42 -0.38 -0.5 -0.53 -0.45
spt20Δ (SC) 0.68 0.7 0.6 1 0.94 0.42 -0.36 -0.45 -0.47 -0.43
spt7Δ (SC) 0.68 0.67 0.58 0.94 1 0.49 -0.32 -0.42 -0.42 -0.4
spt3Δ (SC) 0.44 0.43 0.42 0.42 0.49 1 -0.18 -0.26 -0.21 -0.19
Taf13-deg (SC) -0.42 -0.44 -0.38 -0.36 -0.32 -0.18 1 0.8 0.77 0.73
Taf1-deg (YPD) -0.53 -0.54 -0.5 -0.45 -0.42 -0.26 0.8 1 0.89 0.85
Taf7-deg (YPD) -0.53 -0.55 -0.53 -0.47 -0.42 -0.21 0.77 0.89 1 0.84
Taf13-deg (YPD) -0.46 -0.48 -0.45 -0.43 -0.4 -0.19 0.73 0.85 0.84 1
Spt3/20-deg (SC)
Spt3/7-deg (SC)
Spt3/7-deg (YPD)
spt20Δ (SC)
spt7Δ (SC)
spt3Δ (SC)
Taf13-deg (SC)
Taf1-deg (YPD)
Taf7-deg (YPD)
Taf13-deg (YPD)
0.8
0.4
0.0
−0.4
−0.8
Pearson correlation coefficient

A

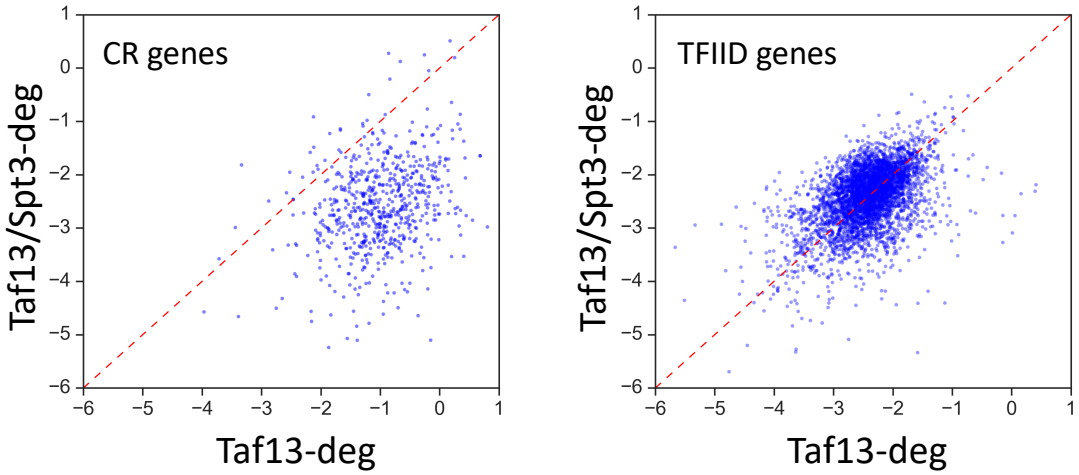
CR genes
TFIID genes
Taf13/Spt3-deg
Taf13-deg
1
0
−1
−2
−3
−4
−5
−6

B

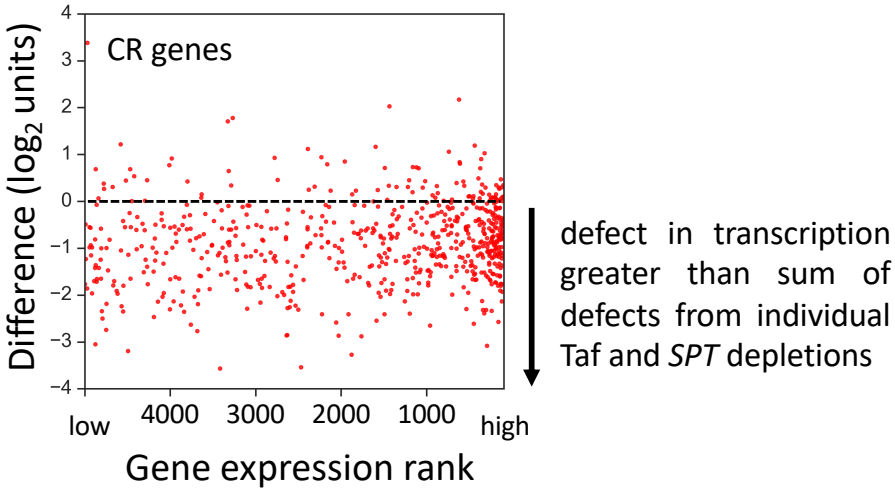
CR genes
Difference (log2 units)
4
3
2
1
0
−1
−2
−3
−4
low
4000
3000
2000
1000
high
Gene expression rank
defect in transcription greater than sum of defects from individual Taf and SPT depletions

A

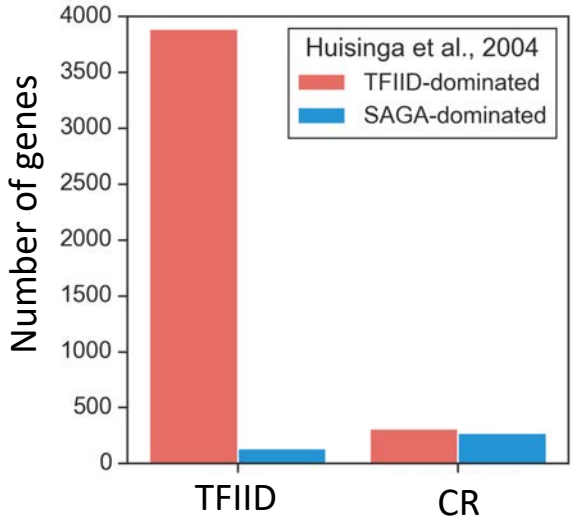
Huisinga et al., 2004
TFIID-dominated
SAGA-dominated
Number of genes
4000
3500
3000
2500
2000
1500
1000
500
0
TFIID
CR

B

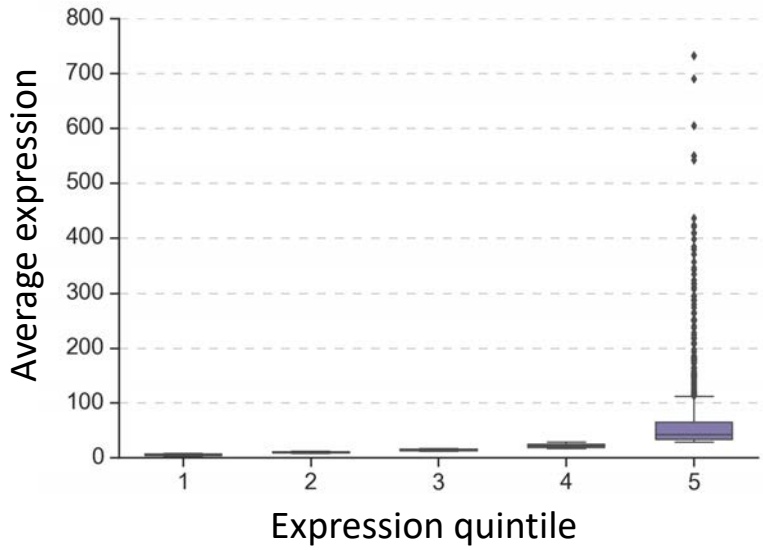
Average expression
800
700
600
500
400
300
200
100
0
1
2
3
4
5
Expression quintile

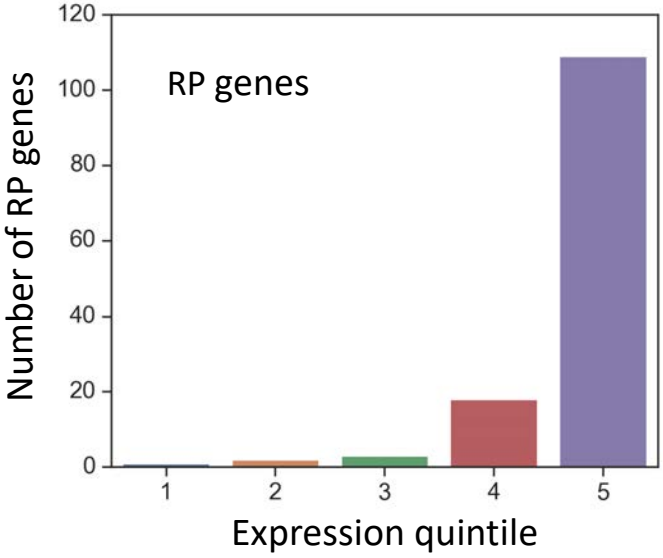
RP genes
Number of RP genes
120
100
80
60
40
20
0
1
2
3
4
5
Expression quintile

A SAGA deletions

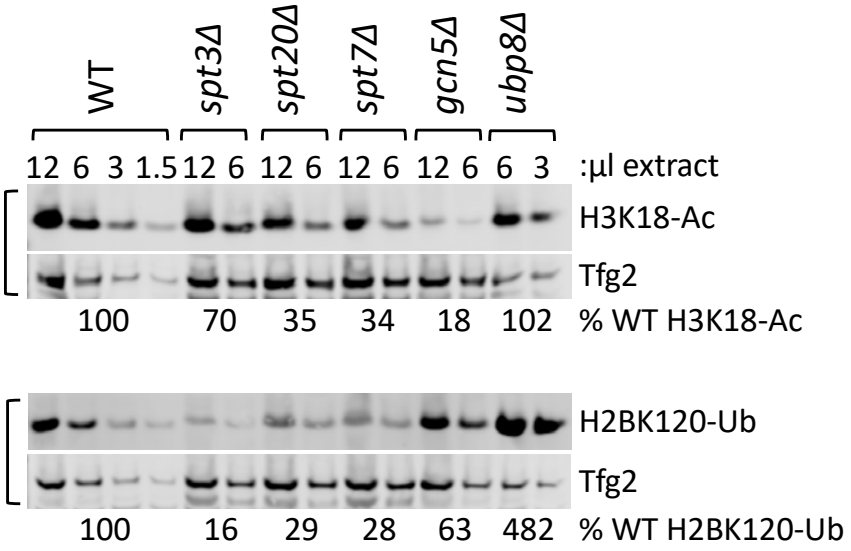

B SAGA degrons

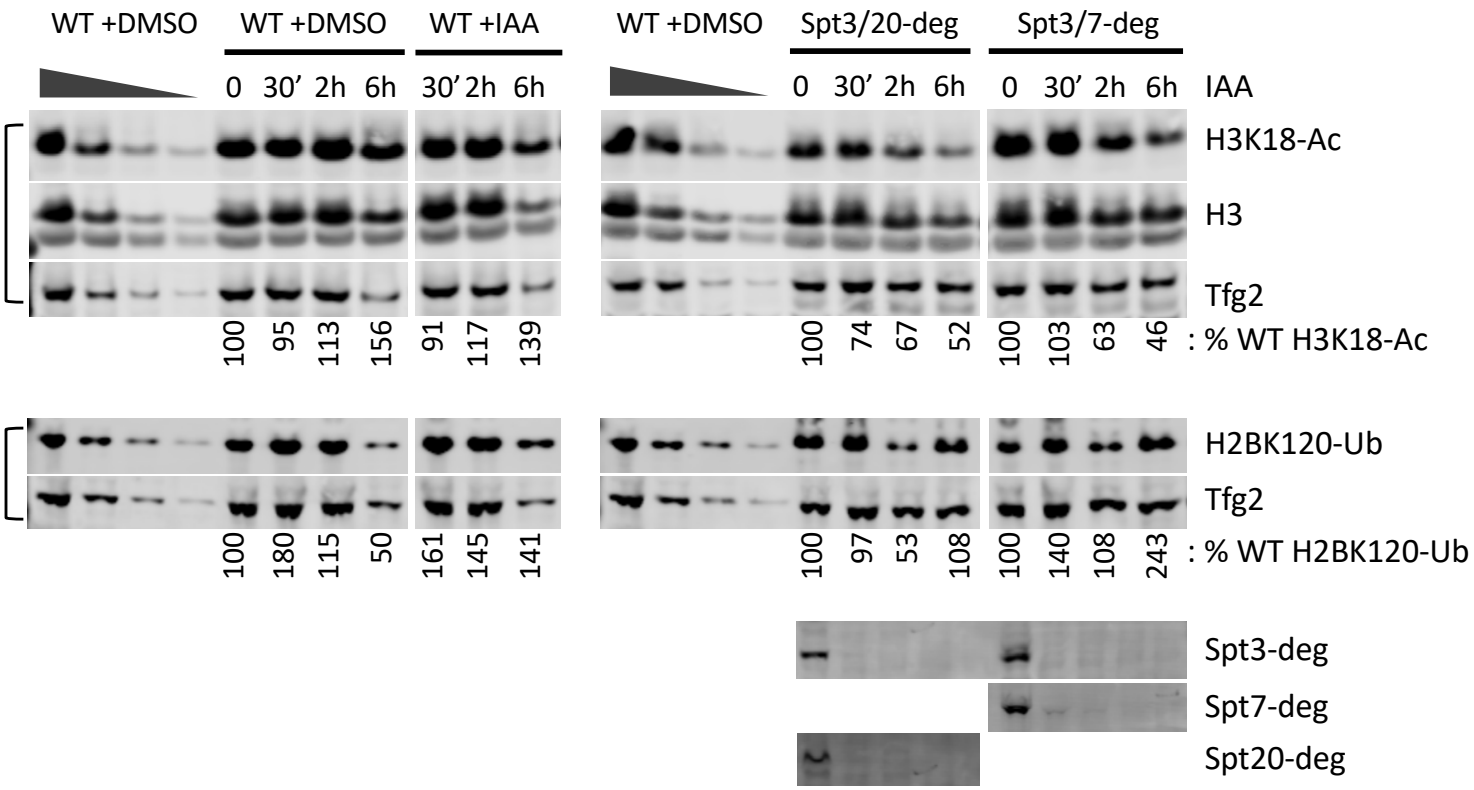

A H3K18-Ac ChIP-seq

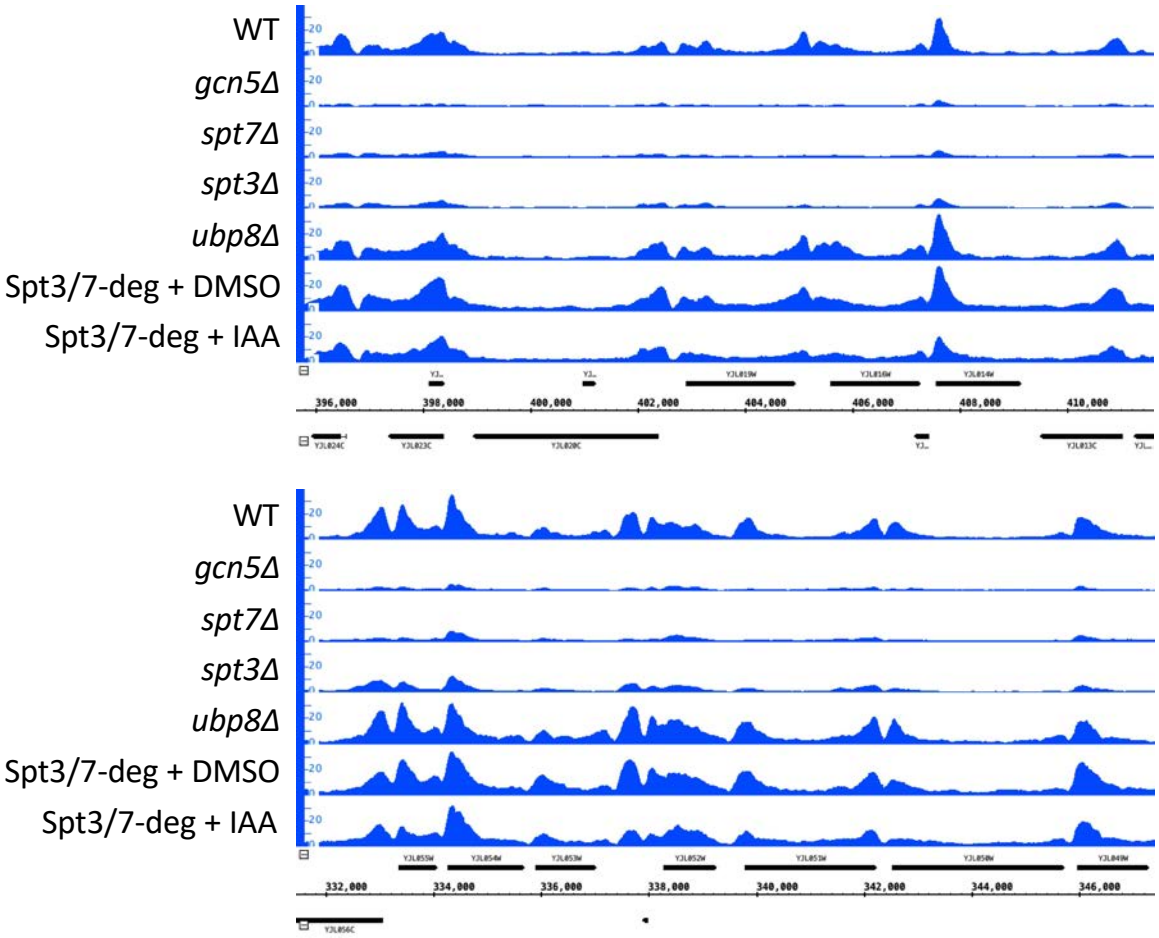

B H3K18-Ac ChIP-seq

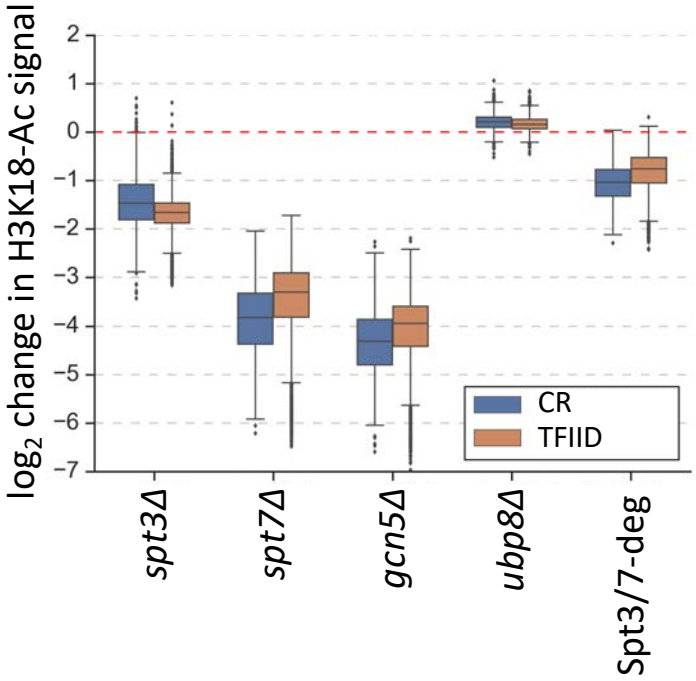

C

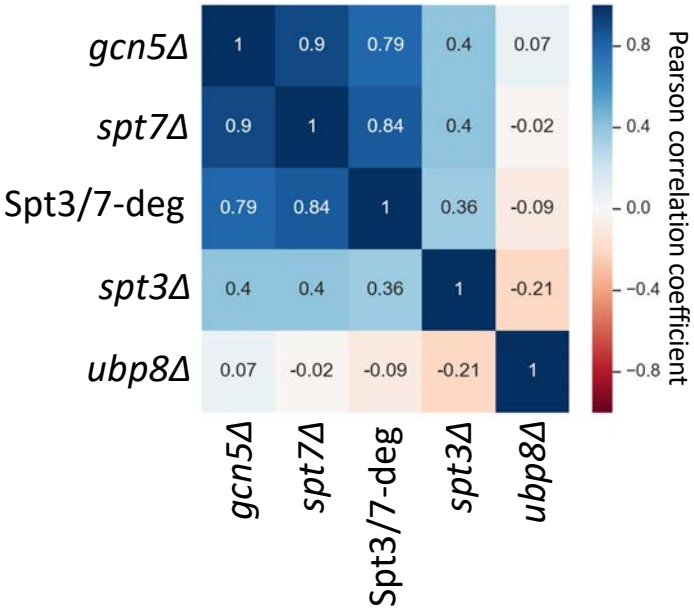

A

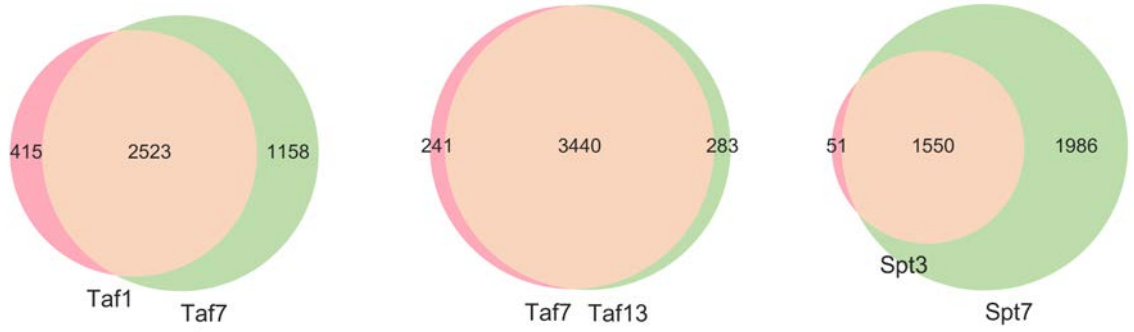
415
2523
1158
Taf1
Taf7
241
3440
283
Taf7
Taf13
51
1550
1986
Spt3
Spt7

B

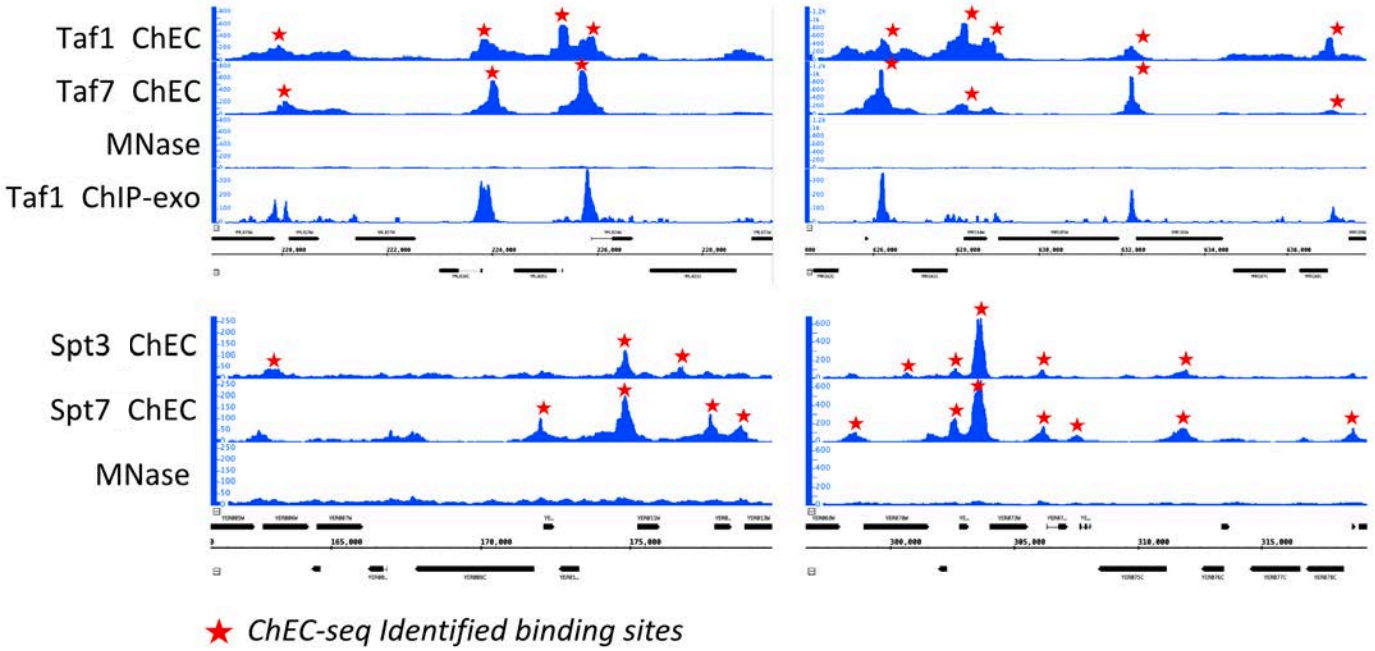
Taf1 ChEC
Taf7 ChEC
MNase
Taf1 ChIP-exo
Spt3 ChEC
Spt7 ChEC
MNase
ChEC-seq Identified binding sites

C

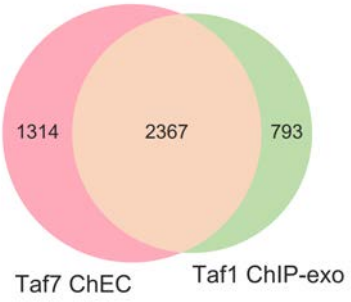
1314
2367
793
Taf7 ChEC
Taf1 ChIP-exo

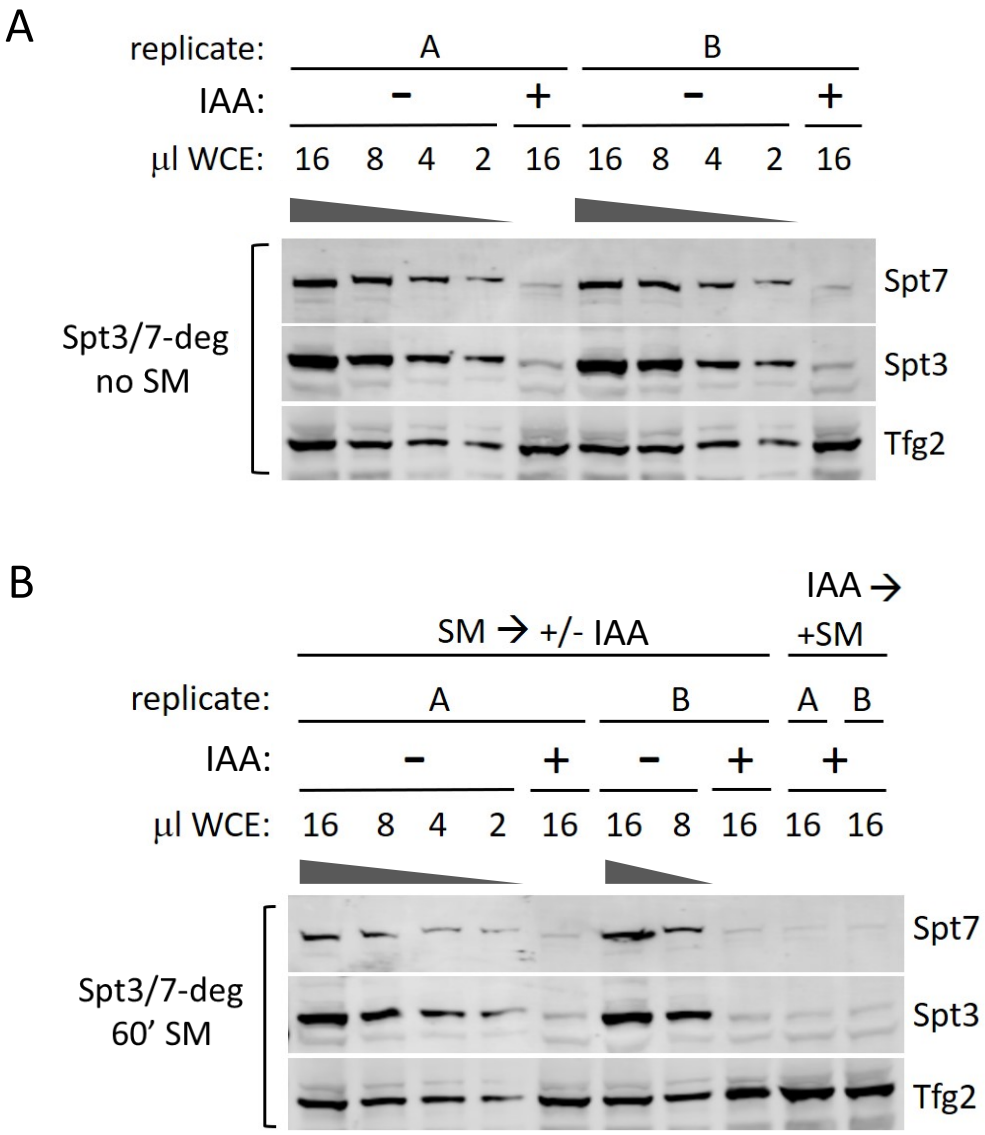
A
replicate:
A
B
IAA:
-
+
-
+
µl WCE:
16 8 4 2 16 16 8 4 2 16
Spt3/7-deg
no SM
Spt7
Spt3
Tfg2
B
IAA →
SM → +/- IAA
+SM
replicate:
A
B
A B
IAA:
-
+
-
+
+
µl WCE:
16 8 4 2 16 16 8 16 16 16
Spt3/7-deg
60' SM
Spt7
Spt3
Tfg2